A comparative study between numerical methods in simulation of cavitating bubbles

Downloaded from: https://research.chalmers.se, 2025-12-04 08:23 UTC

Citation for the original published paper (version of record):
Ghahramani, E., Arabnejad Khanouki, M., Bensow, R. (2019). A comparative study between numerical methods in simulation of cavitating bubbles. International Journal of Multiphase Flow, 111: 339-359. http://dx.doi.org/10.1016/j.ijmultiphaseflow.2018.10.010

N.B. When citing this work, cite the original published paper.

research.chalmers.se offers the possibility of retrieving research publications produced at Chalmers University of Technology. It covers all kind of research output: articles, dissertations, conference papers, reports etc. since 2004. research.chalmers.se is administrated and maintained by Chalmers Library

(article starts on next page)

International Journal of Multiphase Flow xxx (xxxx) xxx

Contents lists available at ScienceDirect

International Journal of Multiphase Flow

journal homepage: www.elsevier.com/locate/ijmulflow

A comparative study between numerical methods in simulation of cavitating bubbles

Ebrahim Ghahramani*, Mohammad Hossein Arabnejad, Rickard E. Bensow

Mechanics and Maritime Sciences, Chalmers University of Technology, Gothenburg 412 96, Sweden

ARTICLE INFO

Article history:
Received 25 April 2018
Revised 7 August 2018
Accepted 16 October 2018
Available online xxx

Keywords:
Cavitation
Eulerian–Lagrangian model
Equilibrium model
Finite mass transfer

ABSTRACT

In this paper, the performance of three different numerical approaches in cavitation modelling are compared by studying two benchmark test cases to understand the capabilities and limitations of each method. Two of the methods are the well established compressible thermodynamic equilibrium mixture model and the incompressible transport equation finite mass transfer mixture model, which are compared with a third method, a recently developed Lagrangian discrete bubble model. In the Lagrangian model, the continuum flow field is treated similar to the finite mass transfer approach, however the cavities are represented by individual bubbles. Further, for the Lagrangian model, different ways to consider how the fluid pressure influences bubble dynamics are studied, including a novel way by considering the local pressure effect in the Rayleigh–Plesset equation. The first case studied is the Rayleigh collapse of a single bubble, which helps to understand each model behaviour in capturing the cavity interface and the surrounding pressure variations. The special differences between the Lagrangian and finite mass transfer models in this case clarify some possible origin for some limitations of the latter method. The second investigated case is the collapse of a cluster of bubbles, where the collapse of each bubble is affected by the dynamics of surrounding bubbles. This case confirms the importance of considering local pressure in the improved form of the Rayleigh–Plesset equation and illustrates the influence of the liquid compressibility for cavity modelling and appropriate capturing of the collapse pressure.

© 2018 Published by Elsevier Ltd.

1. Introduction

Understanding and control of cavitation and its consequences is still a challenge in engineering. In many applications, cavitation is an undesirable phenomenon and it is tried to avoid its occurrence, or at least to minimize its effects. Cavitation erosion causes material loss and degradation of hydraulic systems such as pumps, turbines and ship propellers. Other nuisances from cavitation include issues like noise, vibrations, load variations, and blockage in the machinery. However, it is found a desirable event in some other situations such as ultrasonic cleaning and ultrasonic drug delivery. Therefore, reliable prediction and control of cavitation is of considerable importance in the design of hydraulic and marine systems as well as its application in biomedical treatment and chemical systems.

Computational Fluid Dynamics (CFD) can be a supplement or alternative to experimental measurements. Experimental tests can be very expensive, suffer from scale effects, and give limited information; the latter is a particular problem in cavitating flows where the application of optical measurement techniques is often not possible. In comparison, CFD methods can provide more detailed features of the flow field to have a more comprehensive understanding of the hydrodynamics of cavitation. However, cavitating flows include a vast range of spatial and temporal scales, and sometimes are accompanied by other processes and flow effects that make the modelling and computations challenging. For example, the duration of the final stage of bubble or cavitating vortex collapse is of the order of one microsecond (Franc and Michel, 2006) while the erosion process might take place over the lifetime of a propeller. Also, the normal velocity of the interface can vary from some meters per second for turbomachinery systems to hundreds of meters per second in diesel injector nozzles. Besides that, the peak pressures can reach up to several thousands of bars for a few microseconds during the last stages of cavity collapse. Another parameter to consider is fluid properties, as cavitation does not occur only in water but also in e.g. rocket pumps, the lubricant of bearings (Koop, 2008), diesel injectors, or blood vessels during ultrasound drug delivery. Depending on the fluid properties and pressure differences, sometimes strong shock waves and considerable temperature variations are seen in the domain which means that the compressibility and thermal effects should

* Corresponding author.
E-mail address: ebrahim.ghahramani@chalmers.se (E. Ghahramani).

https://doi.org/10.1016/j.ijmultiphaseflow.2018.10.010
0301-9322/© 2018 Published by Elsevier Ltd.

Please cite this article as: E. Ghahramani et al., A comparative study between numerical methods in simulation of cavitating bubbles, International Journal of Multiphase Flow (2018), https://doi.org/10.1016/j.ijmultiphaseflow.2018.10.010

be considered in the simulation. Considering the issues with sufficient spatial and temporal resolutions as well as the mentioned flow effects, there is no unique CFD approach today that has sufficient performance for every cavitation problem. In fact, current computational capabilities do not allow the resolution of all scales arising in typical cavitating flows except for a few academic cases (Schmidt et al., 2014). Therefore, various numerical methods are being used today, and each of them is applicable or feasible only to a specific group of cavitation problems.

There are different categorizations of cavitation models based on the fundamental assumptions behind them. In one group of models, the two-phase cavitation regime is considered as a single fluid flow which is in mechanical and thermodynamic equilibrium. This equilibrium assumption implies that mass transfer rate at the gas–liquid interface is infinite. These models are mostly implemented in density-based algorithms with different approaches to find the pressure-density relation. For example, Schnerr et al. (2008) and Koop (2008) used an equation of state (EoS) to find the flow pressure. The different phases and their relevant interface are recognised based on the density value at each point and the EoS can be a function of temperature. Kyriazis et al. (2017) used an explicit density-based solver with real fluid thermodynamic properties for n-Dodecane to demonstrate heating effects in bubble collapse cases. When the flow temperature variation is not significant, the EoS can be independent of the temperature which simplifies the pressure-density relations; this is known as barotropic EoS. The barotropic models are implemented in both density-based (e.g. Koukouvinis et al., 2016a) and pressure-based algorithms. Goncalves et al. (2010) compared an incompressible pressure-based solver with a compressible density-based solver with barotropic cavitation models. From the results, it seems necessary to consider fluid compressibility effects to correctly describe the cavity dynamics. The single fluid EoS models do not usually need any empirical parameters; however, the captured liquid–gas interface is rather diffuse in these models and high grid resolutions with very small time steps are needed for adequate prediction of a sharp interface. Furthermore, to correctly capture pressure wave propagation, very small time steps are normally needed in the simulation. Therefore, these models are computationally expensive and they are usually applied to cavitating flows in small scale geometries such as diesel injector nozzle flows.

Another widely used modelling approach is the transport equation based method. Here, similar to the previous approach, the multiphase flow is treated as a homogeneous mixture and one set of continuity and momentum equations is used to calculate the mixture flow. However, a transport equation is solved to capture the liquid–vapour interface. This equation can be developed based on the volume fraction of the two phases (e.g. Singhal et al., 2002 & Bensow and Bark, 2010) or through a level-set method, i.e. expressed based on a signed distance of any point to the interface (e.g. Lauer et al., 2012). Also, the mass transfer between the phases is defined as an explicit source term to the transport equation. Therefore, this approach, known as finite mass transfer rate method (FMT), should incorporate a numerical model to estimate vaporization and condensation rates. Most models that are used in the literature (selectively Schnerr and Sauer, 2001, Merkle et al., 1998 & Kunz et al., 2000) estimate the phase change rate based on a simplified form of the Rayleigh–Plesset equation, in which the second temporal derivative of bubble radius as well as the effect of non-condensable gas are ignored. This simplification may affect the model accuracy; Ye and Li (2016) showed that the bubble growth rate can become greatly reduced if the bubble-bubble interaction and second-order derivative in the Rayleigh–Plesset equation are considered. To improve the model accuracy, however, some empirical constants are implemented in these models which should be tuned for each different simulation to adjust the mass transfer rate. Such uncertainty of model constants is one of the limitations of the finite mass transfer approach. A recent study by Koukouvinis and Gavaises (2015) showed that even with the finite mass transfer approach consistent results can be achieved by theoretically increasing the transfer rates to infinity. The transport equation method is commonly implemented in pressure-based algorithms and the pure fluids are usually assumed to be incompressible; there are, however, a few studies in which the fluid compressibility is taken into account. For example, Koukouvinis et al. studied the expansion and collapse of a single bubble subject to gravity (Koukouvinis et al., 2016b) and in the vicinity of a free surface (Koukouvinis et al., 2016c). However, they ignored the mass transfer rate in the simulation. Also, Yakubov et al. (2015) investigated the effect of fluid compressibility in pressure-based solvers using the finite mass transfer approach. This study shows that considering fluid compressibility in the pressure correction equation may lead to ill-conditioned matrices of coefficients which can cause numerical issues for steady-state simulations or transient simulations with large time steps. From the results, it can also be inferred that the cavitation patterns are very similar for compressible and incompressible simulations. Therefore, for the large scale problems, such as cavitating ship propellers and turbines, it is more common to use incompressible transport equation models as they are less computationally expensive and can give rather satisfactory results using larger time steps, as compared to equilibrium-based models. However, due to simplifications in the mass transfer rate model as well as the grid resolution dependency of the transport equation, cavity structures smaller than the grid size, such as cavitation nuclei and bubbles, or sparse clouds of bubbles, are not well treated using these approaches. Accurate simulation of such structures and their violent collapses and fast rebounds are very important in accurate prediction of cavitation erosion.

Discrete bubble model (DBM) is another approach in which the cavity structures are tracked in a Lagrangian framework while the continuum flow is still calculated using Eulerian governing equations. In other words, cavity structures are considered as individual bubbles, and groups of bubbles, or parcels of them, are tracked by solving the Lagrangian equations of motion. Different numerical studies in the literature show the potential of this method to resolve cavitation phenomenon. Giannadakis et al. (2008), for example, studied the predictive capability of a stochastic Lagrangian model accounting for the onset and development of cavitation inside diesel nozzle holes. Since different flow forces on cavities are implemented directly in the transport equation and bubble size variation is represented using a more accurate form of the Rayleigh–Plesset equation, the Lagrangian approach can give a more realistic estimation of cavitation dynamics as compared to the transport equation approach. Abdel-Maksoud et al. (2010) compared Euler-Euler and Euler-Lagrange methods, and showed that only Lagrangian models are able to describe correctly the bubble behaviour in vortices. In this method, the small subgrid scale structures and nuclei can be resolved which is crucial in cavity collapse and rebound estimation as well as erosion prediction. Also, it allows to take into account inhomogeneous and transient water-quality effects (Yakubov et al., 2013).

To have a more physical representation of the cavity dynamics in DBM, various interactions between cavity structures should be modelled appropriately in the solution algorithm. These interactions include, but are not limited to, different flow forces on bubble trajectory as well as its dynamics, turbulence effect on bubble motion and break-up, bubble-bubble interaction and the bubble contribution on mixture properties and surrounding pressure. However, the Lagrangian models can be computationally expensive when the number of bubbles is large. Besides that, they are limited in representation of large and non-spherical vapour structures. To overcome these limitations, hybrid multi-scale mod-

Please cite this article as: E. Ghahramani et al., A comparative study between numerical methods in simulation of cavitating bubbles, International Journal of Multiphase Flow (2018), https://doi.org/10.1016/j.ijmultiphaseflow.2018.10.010

els are being developed in which the large cavities are represented using a transport equation model while the small scale structures are tracked in the Lagrangian framework. For example, Hsiao et al. (2017) developed a multi-scale approach through coupling of the level-set method with a DBM approach to capture the sheet cavitation formation and development, unsteady breakup, and bubble cloud shedding on a hydrofoil. In another recent study by the current authors (Ghahramani et al., 2018), the DBM model is coupled with the FMT model based on a direct transition between Eulerian structures and Lagrangian bubbles. The concept of multi-scale hybrid Eulerian–Lagrangian solvers is a novel approach to simulate multiphase flows in large scale applications in which effective small scale details need to be resolved sufficiently. This method has proven to be a suitable option to simulate atomizing gas–liquid flows as well (e.g. Ström et al., 2016). A key factor in developing such solvers is the correct and smooth transition between Lagrangian and Eulerian structures (Ghahramani et al., 2017 & Ghahramani et al., 2018).

In this study, an Eulerian–Lagrangian cavitation model based on the coupling of an Eulerian finite mass transfer model and a Lagrangian model is presented and its capability to estimate the dynamics of collapsing bubbles is validated with theoretical and numerical benchmark studies. Here, the vapour–liquid mixture properties is obtained based on a volume fraction methodology, but in which cavities are tracked in the Lagrangian framework rather than solving an Eulerian transport equation. In the general application of the solver, the large cavities are tracked in the Eulerian framework and there is a transition algorithm between Eulerian and Lagrangian frameworks; however, in the test cases of this study, emphasise is on the Lagrangian model performance in prediction of bubble collapse dynamics and its effect on the continuum pressure through the Eulerian–Lagrangian coupling. Further, the general Rayleigh–Plesset equation, that describes the relation between flow pressure and bubble size, is improved to have a more appropriate representation of local flow pressure effect on bubble dynamics.

Although cavitating flows in general consist of different complex structures such as sheet and cloud cavities, nuclei and the dynamics of bubbles often play a crucial role for the nuisance of cavitation. Thus, the correct representation of the effects of bubble cavitation, and cluster of bubbles, is very important for detailed assessment of cavitation. Besides that, there are special problems in which the structures are only a group of bubbles. For example, in ultrasonic drug delivery bubbles are considered as suitable vehicles to carry drugs as they can be circulated in the body without loosing the drug near healthy tissues, while near the infected tissues they can release the drug via a violent collapse which is triggered by ultrasonic pressure waves (Ibsen et al., 2013). Therefore, the study of bubbly flows and bubble effects have been the subject of different studies in literature (selectively Tiwari et al., 2015, Mattson and Mahesh, 2012 & Wang and Brennen, 1999). In such problems, the Lagrangian approach seems to be the appropriate option which can give detailed information on bubble dynamics, although the other methods may be used if the bubbles may be resolved.

The first test case, thus, is a single bubble collapse in which the three approaches are compared: the compressible EoS, the incompressible FMT, and the Lagrangian approach. For this case, an analytical solution is available, and the predicted bubble collapse behaviour and the surrounding pressure can be assessed in detail. In the second test, the collapse of a cluster of bubbles is investigated; previously studied by Schmidt et al. (2011). Here, no exact solution is available but only comparison between the methods can be made. In addition to validating the Lagrangian model and the improved Rayleigh–Plesset equation, the performance of the Eulerian finite mass transfer model is studied in detail and the effect of various parameters in this method including empirical constants are investigated, which helps to have a better understanding of its behaviour and possible source of deficiencies for future improvements. All simulation models are developed in the open source C++ package OpenFOAM (OpenFoam, 2018); for the Lagrangian model this involves improving the interPhaseChangeFOAM solver and coupling it with a Lagrangian library, which is an improved version of an available Lagrangian model in OpenFOAM.

In the following sections, the three numerical models are described first. Then, the performance of the three models are compared in simulating the single bubble collapse and the strength and deficiency of each method are discussed. In this part, the effects of mass transfer model empirical constant and simulation time step in capturing the flow physics is investigated. After that, the models are compared in simulating the collapse of a cluster of bubbles, where the effect of neighbouring bubbles and relative pressure pulses play an important role in the collapse behaviour. The paper is then concluded with recommendations for future development of finite mass transfer and Lagrangian models.

2. Numerical methods

2.1. Compressible equilibrium EoS model

In this study, the governing equations of the compressible model are the Euler equations, which include continuity, momentum, and energy equations, similar to previous studies of Sezal (2012) and Koop (2008). Due to the dominance of inertia effects within the considered benchmark cases, viscous effects can be neglected. The equations are given by

$$\frac{\partial \vec{q}}{\partial t} + \frac{\partial F_i(\vec{q})}{\partial x_i} = 0, \tag{1}$$

where $\vec{q}$ is the vector of conserved quantities defined as

$$\vec{q} = \begin{bmatrix} \rho \\ \rho u_1 \\ \rho u_2 \\ \rho u_3 \\ \rho E \end{bmatrix}, \tag{2}$$

and $F_i(\vec{q})$ is the physical flux in coordinate direction x_i, given by

$$F_i(\vec{q}) = \rho u_i \begin{bmatrix} 1 \\ u_1 \\ u_2 \\ u_3 \\ E \end{bmatrix} + p \begin{bmatrix} 0 \\ \delta_{1i} \\ \delta_{2i} \\ \delta_{3i} \\ u_i \end{bmatrix} \tag{3}$$

In these equations, ρ is the fluid density, u_i is the velocity vector, p is the pressure, δ_{ij} denotes the Kronecker symbol, and E is the specific total energy which is the sum of the specific internal energy and the specific kinetic energy. The Euler equations are solved with the suitable temperature dependent equations of state for each phase.

In two-phase water-vapour flows, three possible states may occur: pure liquid, pure vapour, and mixture. If the calculated density is higher than the liquid saturation density, the fluid is assumed to be pure liquid. The liquid phase is then described by the modified Tait EoS (Saurel and Abgrall, 1999), given by

$$p = K_0 \left[\left(\frac{\rho}{\rho_{l,sat}(T)} \right)^N - 1 \right] + p_{sat}(T), \tag{4}$$

where K_0 is a liquid dependent constant and $\rho_{l,sat}$ is the saturated liquid density at temperature T. Since the density of water is approximately constant, the temperature can be obtained from the

Table 1
Equilibrium model parameters.

N	K_0	$C_{vl}\,(J/kgK)$	$C_{vv}\,(J/kgK)$	$T_0\,(K)$	$e_{l0}\,(J/kg)$	$R\,(J/kgK)$	$L_v(T_0)\,(J/kgK)$
7.15	3.3×10^8	4180	1410.8	273	617	461.6	2.753×10^6

caloric EoS (Koop, 2008 & Saurel et al., 1999), which is an approximation of the complete form of internal energy equation, as

$$T = \frac{e - e_{l0}}{C_{vl}} + T_0, \tag{5}$$

where e is the internal energy of the fluid and e_{l0} is the liquid internal energy at reference temperature of T_0. Also, C_{vl} is the liquid specific heat at constant volume. When the density drops below the vapour saturation density, the fluid is assumed to be pure vapour. The perfect gas law is used to describe the pure vapour phase,

$$p = \rho RT. \tag{6}$$

Here, R is the specific gas constant and the temperature is obtained using the caloric EoS,

$$T = \frac{e - e_{l0} - L_v(T_0)}{C_{vv}} + T_0. \tag{7}$$

In this relation, $L_v(T0)$ is latent heat of vaporization at the reference temperature (T_0) and C_{vv} is the vapour specific heat at constant volume. With the thermodynamic equilibrium assumption, the mixture pressure can be considered equal to saturation pressure. Here, the temperature is calculated using the mixture internal energy as

$$T = \frac{\rho(e - e_{l0}) - \alpha_v \rho_{v,sat} L_v(T_0)}{\alpha_v \rho_{v,sat} C_{vv} + (1-\alpha_v)\rho_{l,sat} C_{vl}} + T_0, \tag{8}$$

where $\rho_{v,\,sat}$ is the saturated vapour density at temperature T and α_v is the vapour volume fraction, computed from the mixture density as

$$\alpha_v = \frac{\rho - \rho_{l,sat}}{\rho_{l,sat} - \rho_{v,sat}}. \tag{9}$$

The parameters in Eqs. (4)–(8) are given in Table 1. The saturated values of pressure, p_{sat}, and liquid and vapour saturated density, $\rho_{l,\,sat}$ and $\rho_{v,\,sat}$, in the equations are obtained from IAPWS-IF97 library (Wagner and Kretzschmar, 2008).

In this model, the compressibility of both liquid and vapour phases is taken into account, which makes it capable of capturing possible shock and pressure waves in a cavitating flow. The model has been implemented as a density-based solver in OpenFOAM (Eskilsson and Bensow, 2012). The numerical flux is evaluated by solving the approximate Riemann problem using HLLC-AUSM low-Mach Riemann solver (Koop, 2008). Second order accuracy in space is achieved by piece-wise linear reconstruction with the limiter function of Venkatakrishnan (Venkatakrishnan, 1995). The solution is advanced in time using a second order explicit low storage Runge–Kutta scheme.

2.2. Incompressible finite mass transfer model

In this model, the vapour and liquid phases are treated as a single mixture fluid and the continuity and Navier–Stokes equations are solved to calculate the mixture flow. Here the flow is considered as incompressible and isothermal, motivated by the balance of computational cost and model accuracy for the intended applications as described above, but a similar framework can be developed for compressible flows.

Although the pure liquid and pure vapour are considered as incompressible, the mixture density varies based on volume fraction of the immiscible phases and hence the continuity equation is given by

$$\frac{\partial u_i}{\partial x_i} = \left(\frac{1}{\rho_l} - \frac{1}{\rho_v}\right)\dot{m}. \tag{10}$$

The RHS term is the effect of vaporization and condensation, where $\dot{m}$ is the rate of mass transfer between phases, ρ_l is the liquid density and ρ_v is the vapour density. Further, the Navier–Stokes equation is

$$\frac{\partial(\rho_m u_i)}{\partial t} + \frac{\partial\left(\rho_m u_i u_j\right)}{\partial x_j} = \frac{\partial \tau_{ij}}{\partial x_j} + \rho_m g_i. \tag{11}$$

In this equation, τ_{ij} is the stress tensor and ρ_m is the mixture density. They are defined as

$$\tau_{ij} = -p\ \delta_{ij} + \mu_m\left(\frac{\partial u_i}{\partial x_j} + \frac{\partial u_j}{\partial x_i} - \frac{2}{3}\frac{\partial u_k}{\partial x_k}\delta_{ij}\right), \tag{12}$$

$$\rho_m = \alpha\rho_l + (1-\alpha)\rho_v, \tag{13}$$

where μ_m is the mixture dynamic viscosity, given by

$$\mu_m = \alpha\mu_l + (1-\alpha)\mu_v, \tag{14}$$

and α is the liquid volume fraction that specifies the relative amount of liquid in a control volume. In the volume fraction based incompressible finite mass transfer models, this quantity is calculated by solving a scalar transport equation given as

$$\frac{\partial \alpha}{\partial t} + \frac{\partial(\alpha u_i)}{\partial x_i} = \frac{\dot{m}}{\rho_l}. \tag{15}$$

To close the above set of equations, the mass transfer rate, $\dot{m}$, should be determined. There are many numerical models proposed in literature to estimate this term and most of them are based on a simplified form of the Rayleigh–Plesset equation (later given in Eq. (24)) in which the second order derivative term as well as dissolved gas pressure, surface tension and viscous forces are neglected. The Schnerr-Sauer model (Schnerr and Sauer, 2001; OpenFoam, 2018) has been used quite often in literature (e.g. Asnaghi et al., 2017) and has been proven to give reasonably satisfactory results for a range of applications. This model is used in the current study, and the vaporization and condensation rates are given by

$$\dot{m}_c = C_c\alpha(1-\alpha)\frac{3\rho_l\rho_v}{\rho_m R_B}\sqrt{\frac{2}{3\rho_l|p-p_{threshold}|}}\max(p-p_{threshold},0),$$
$$\dot{m}_v = C_v\alpha(1+\alpha_{Nuc}-\alpha)\frac{3\rho_l\rho_v}{\rho_m R_B}\sqrt{\frac{2}{3\rho_l|p-p_{threshold}|}}\min(p-p_{threshold},0), \tag{16}$$

where $\dot{m}_c$ and $\dot{m}_v$ are the rates of condensation and vaporization, respectively. In the above equations, R_B and α_{Nuc} are the generic radius and volume fraction of bubble nuclei in the liquid which are obtained from

$$\alpha_{Nuc} = \frac{\frac{\pi n_0 d_{Nuc}^3}{6}}{1+\frac{\pi n_0 d_{Nuc}^3}{6}}, \tag{17}$$

$$R_B = \sqrt[3]{\frac{3}{4\pi n_0}\frac{1+\alpha_{Nuc}-\alpha}{\alpha}}, \tag{18}$$

where n_0 and d_{Nuc} are user defined parameters corresponding to the number of nuclei per cubic meter and the nucleation site diameter, respectively. Also, C_c and C_v are the condensation and vaporization rate coefficients in OpenFOAM (OpenFoam, 2018), and

$p_{threshold}$ is a threshold pressure at which the phase change is assumed to happen, usually considered as the vapour pressure of the fluid. As the overall combination of these values only influences the mass transfer rate as a constant coefficient, in this study only the vaporization and condensation rate coefficients (C_v and C_c) are modified and the fluid properties as well as model parameters are kept constant. The number of nuclei per cubic meter (n_0) is assumed to be 10^8 and the nucleation site diameter (d_{Nuc}) is set to $10^{-4}m$.

In the finite mass transfer solver, the pressure and velocity equations are coupled using a PIMPLE algorithm. This algorithm is a merge of the SIMPLE (Patankar and Spalding, 1983) and PISO algorithms, where the PISO loop is complemented by an outer iteration loop, see e.g. Barton (1998) for different ways to merge PISO and SIMPLE procedures. For the single bubble test case, at each time step, one outer SIMPLE loop is performed, and in each SIMPLE loop at least three PISO loops are performed. For the bubble cluster simulation, four outer SIMPLE loops are performed, and in each SIMPLE loop four PISO loops are performed. A first order implicit time scheme is used for time discretization. The momentum equation convection terms are discretized using Gaussian linear upwind differencing scheme while the convective terms of the volume fraction scalar equation is discretized by Gaussian TVD schemes with the van Leer limiter.

One feature of the mass transfer approach, similar to the equilibrium EoS method, is that it treats the structures that are smaller than the grid size as a homogeneous mixture, therefore sparse vapour clouds or sub-grid inhomogeneity in cavitation clouds are not well treated. An extremely high mesh resolution would be required to resolve the small individual cavitation bubbles, which is not feasible in engineering applications. In addition, during the last steps of the cavity collapse and early stages of its rebound, the cavity size changes very rapidly and the bubble inertia becomes more important. However, in the simplified mass transfer model the bubble inertia, corresponding to second order derivative term in the Rayleigh–Plesset equation, is ignored and this approach cannot fully resolve cavity collapse and rebound. The Eulerian–Lagrangian model, however, is potentially able to take into account the cavity inertia and is less dependent on grid resolution.

2.3. Eulerian–Lagrangian model

In this model the cavities are treated as discrete Lagrangian bubbles in an ambient Eulerian continuous flow. At each time step, the Eulerian equations are solved first, then the bubbles are tracked by solving a set of ordinary differential equations along the bubble trajectory, after which the Eulerian vapour fraction is updated based on the new bubble positions and radii. The Eulerian governing equations are the continuity and Navier–Stokes equations as described for the finite mass transfer model (Eqs. (10) and (11)) and the Lagrangian equations for tracing individual bubbles are given by

$$\frac{dx_{b,i}}{dt} = u_{b,i},$$
$$m_b \frac{du_{b,i}}{dt} = F_d + F_l + F_a + F_p + F_b + F_g. \tag{19}$$

The RHS of the second equation includes various forces exerted on the bubbles which are, from left to right, sphere drag force (Liu et al., 1993), Saffman–Mei lift force (Mei, 1992), added mass, pressure gradient force, buoyancy force, and gravity. Explicit implementation of flow forces is an advantage of the Lagrangian model which gives the opportunity to consider different flow effects on cavity behaviour, but it also means that the representation is dependent on the accuracy of available models for these effects. The forces typically depend on the bubble size.

To find the bubble size variation due to surrounding flow, consider a spherical vapour bubble with radius R in an incompressible Newtonian fluid, Fig. 1. Neglecting the mass transfer through the interface, the liquid velocity is equal to the interface velocity, $u(R,t) = \dot{R}$. Also, ignoring the gravity effect, the pressure on the bubble interface is given by (Franc and Michel, 2006)

$$p_R = p_v + p_{g0}\left(\frac{R_0}{R}\right)^{3\gamma} - 2\frac{\sigma}{R} + 2\mu\frac{\partial u}{\partial r}|_{r=R}. \tag{20}$$

In this relation, p_v is the vapour pressure. The second term is the dissolved gas pressure in which p_{g0} and R_0 are the initial gas pressure and radius. The third term is the surface tension stress in which σ is the surface tension coefficient, and the last term denotes the viscous stress on the bubble surface. In addition to the mentioned simplifications, we assume spherical symmetry around the bubble. Then the flow continuity and momentum equations are simplified as (Franc and Michel, 2006)

$$u(r,t) = \dot{R}\frac{R^2}{r^2}, \tag{21}$$

$$\frac{\partial u}{\partial t} + u\frac{\partial u}{\partial r} = -\frac{1}{\rho}\frac{\partial p}{\partial r}. \tag{22}$$

Substituting Eq. (21) into Eq. (22) gives

$$\ddot{R}\frac{R^2}{r^2} + 2\dot{R}^2\left(\frac{R}{r^2} - \frac{R^4}{r^5}\right) = -\frac{1}{\rho}\frac{\partial p}{\partial r}. \tag{23}$$

This equation can simply be integrated between any two points on a radial line from bubble interface to the infinity. If the interface ($r = R$) and infinity ($r = \infty$) are chosen as integration end points, then considering the relative boundary conditions at interface (Eq. (20)) and infinity, the well-known Rayleigh–Plesset equation is achieved as (Franc and Michel, 2006; Brennen, 2013; Plesset and Prosperetti, 1977),

$$\rho\left(R\ddot{R} + \frac{3}{2}\dot{R}^2\right) = p_v - p_\infty + p_{g0}\left(\frac{R_0}{R}\right)^{3\gamma} - 4\mu\frac{\dot{R}}{R} - \frac{2\sigma}{R}, \tag{24}$$

where p_∞ denotes the pressure at infinity. An inherent assumption in this equation is that the bubble is located in a completely unbounded spherically symmetric infinite domain. However, in most real case applications this assumption will not hold, as the bubble is surrounded by other cavity structures or may be confined within flow boundaries. Therefore it is more useful to take the integration between the interface and another nearby point. If the second point is chosen at $r = 2R$, then we achieve a *localized* form of Rayleigh–Plesset equation as

$$\rho\left(\frac{1}{2}R\ddot{R} + \frac{17}{32}\dot{R}^2\right) = p_v - p_{2R} + p_{g0}\left(\frac{R_0}{R}\right)^{3\gamma} - 4\mu\frac{\dot{R}}{R} - \frac{2\sigma}{R}, \tag{25}$$

where p_{2R} denotes the pressure at $r = 2R$. In this study, the time-step adaptive second-order Rosenbrock method is implemented to solve the Rayleigh–Plesset equation numerically (see e.g. Shampine and Reichelt (1997) for a description of this approach).

To consider the bubble effects on the continuous Eulerian field, the continuous flow is considered as a single fluid mixture flow, similar to the finite mass transfer approach. However, instead of solving the vapour transport equation, the volume fraction is calculated from the Lagrangian bubble distribution. In other words, at each time step the α value of each cell is obtained from bubble cell occupancy. The bubble cell occupancy for a cell is obtained based on the relative volume of the cell that is occupied by the bubble(s). This calculation includes a loop over all bubbles inside the cell and summing up the volume of these bubbles and dividing the total volume by the cell volume. Then this relative value is used to define vapour volume fraction, α, which is used to find the

Please cite this article as: E. Ghahramani et al., A comparative study between numerical methods in simulation of cavitating bubbles, International Journal of Multiphase Flow (2018), https://doi.org/10.1016/j.ijmultiphaseflow.2018.10.010

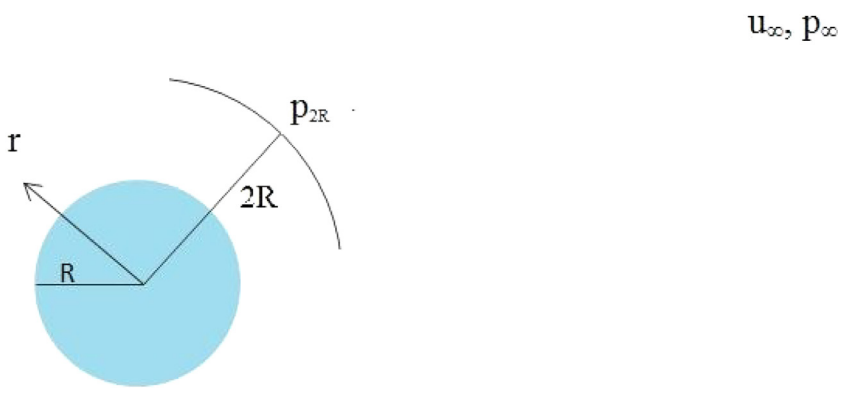

Fig. 1. Single bubble in infinite domain.

mixture properties from Eqs. (13) and (14). Hsiao et al. (2017) used a similar approach to consider bubble contributions in the mixture properties for a multi-scale Eulerian–Lagrangian model. Therefore, in this method the Eulerian continuity and momentum equations are the same as for the incompressible finite mass transfer model. Also, the continuity equation source term is obtained using the Schnerr–Sauer model. It is possible to calculate the phase change source term from bubble size and distribution variation directly, however the intention is to use the Lagrangian approach coupled to a FMT solver; thus to compare the effect of Eulerian cavity transport equation to Lagrangian distribution, in this study the continuity equation is solved in a similar way to the previous method. At each time step, the continuity and Navier–Stokes equations (Eqs. (10) and (11)) are solved first and the updated pressure and velocity field are used to solve the Lagrangian transport equation (19) and Rayleigh–Plesset equation. The updated bubble size and distribution are then used to update the volume fraction values to obtain the new mixture properties for the next time step. The solution algorithm for the Eulerian equations and the equation discretizations for this model are exactly the same as for the finite mass transfer model.

The Lagrangian model that is used in this study is a special version of the hybrid Eulerian mixture- Lagrangian bubble solver that has been introduced in a recent study (Ghahramani et al., 2018). In the current model all of the cavities are treated as Lagrangian bubbles, but in the general form of the hybrid solver, large cavities are represented using the FMT approach and the small structures are tracked as Lagrangian bubbles. For stability reasons and to have the solutions of both FMT and Lagrangian parts being more compatible with each other, it was decided to have similar formula for the continuity equation source terms in the solver and it is the reason to use the Schnerr-Saur model for calculation of the mass transfer source in the Lagrangian approach.

3. Single bubble collapse

The collapse of a single bubble is a benchmark test case that has been widely used for primary validation of different numerical models in literature. Here, the collapse of a vapour bubble in an infinite medium with atmospheric pressure is simulated and the effects of viscosity, non-condensable gas, and surface tension are ignored. This problem is also known as *Rayleigh bubble collapse* and can be solved analytically up to the collapse time. As described by Franc and Michel (2006), the collapse time of the bubble, also known as the Rayleigh time, is given by

$$\tau_R = 0.915 R_0 \sqrt{\frac{\rho}{p_\infty - p_v}}. \tag{26}$$

Further, by integrating the Rayleigh–Plesset equation, the collapse rate is obtained as

$$\frac{dR}{dt} = -\sqrt{\frac{2}{3}\frac{p_\infty - p_v}{\rho}\left(\frac{{R_0}^3}{R^3} - 1\right)}. \tag{27}$$

From this relation, the bubble radius profile can be calculated analytically. The pressure distribution around the bubble is determined from Eq. (23) as

$$\Pi(r) = \frac{p(r) - p_\infty}{p_\infty - p_v} = \frac{R}{3r}\left(\frac{{R_0}^3}{R^3} - 4\right) - \frac{R^4}{3r^4}\left(\frac{{R_0}^3}{R^3} - 1\right). \tag{28}$$

Here, we consider the case where initial bubble radius is 0.4 mm and the flow is assumed to be initially at rest. The initial pressure around the bubble has a Laplacian distribution according to Eq. (23) while the pressure inside is $p_v = 2,320$ Pa. Also, the liquid volume fraction is set to 0.01 inside the bubble and equal to 1 outside. Considering the spherical symmetry of the flow field, only an asymmetric wedge mesh with an angle of five degrees is created (Fig. 2a). The far field boundary is located at 0.5 m from the bubble centre, with a fixed atmospheric pressure (10^5 Pa) and zero gradient conditions for liquid volume fraction and velocity. The total domain is discretized with 5000 cells, including 100 points in the radial direction. The initial bubble is well resolved by 20 cells in the radial direction and 50 cells in the circumferential direction. The generated grid with the initial pressure field is depicted in Fig. 2b; it is radially uniform inside the bubble. For the Eulerian–Lagrangian model, instead of liquid volume fraction initialization, a 0.4 mm bubble is injected at the first time step and the corresponding liquid volume fraction is calculated from bubble cell occupancy. The liquid and vapour densities are assumed to be $\rho_l = 1000$ kg m^{-3} and $\rho_v = 0.01389$ kg m^{-3}, and the corresponding dynamic viscosity values are set as $\mu_l = 0.001$ kg m^{-1} s^{-1} and $\mu_v = 10^{-5}$ kg m^{-1} s^{-1}. The solution time step is set to 5×10^{-9} s for incompressible simulations and 1×10^{-10} s (corresponding to CFL number of 0.32) for the equilibrium model. Therefore, for the incompressible simulations we have $\Delta t/\tau_R = 1.35 \times 10^{-4}$, and for the compressible simulation $\Delta t/\tau_R = 2.7 \times 10^{-6}$. However, larger time steps are also used for time-step dependency studies. In the following sections, the results of each model in solving this problem are compared with the theoretical solution.

3.1. Equilibrium model result

The numerical evolution of bubble radius with time is compared with the exact analytical solution in Fig. 3. In this plot, the radius and the evolution time are non-dimensionalized by initial radius and Rayleigh collapse time, respectively. Since the bubble interface may not be perfectly sharp at all time steps, R is the

Please cite this article as: E. Ghahramani et al., A comparative study between numerical methods in simulation of cavitating bubbles, International Journal of Multiphase Flow (2018), https://doi.org/10.1016/j.ijmultiphaseflow.2018.10.010

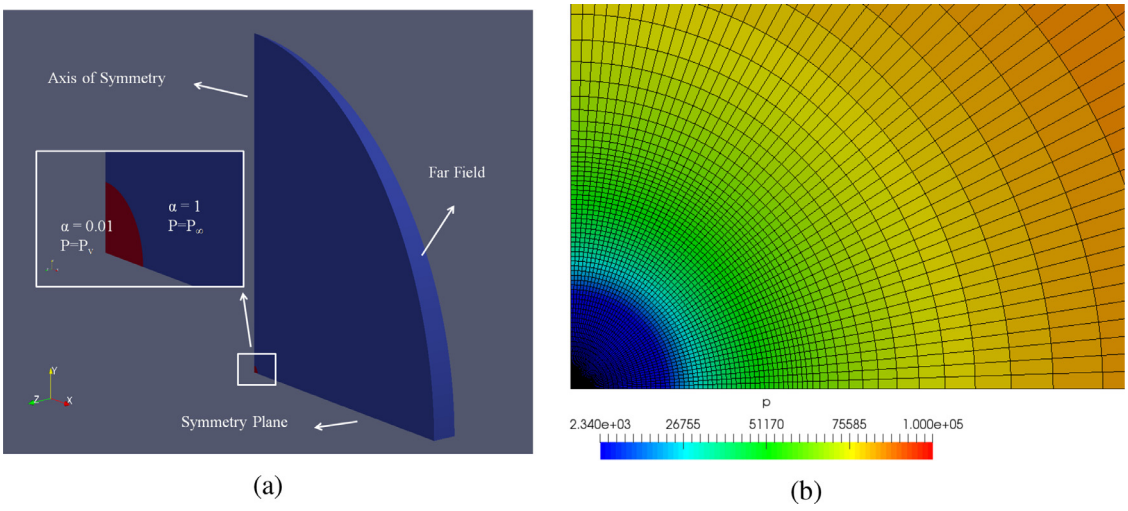

Fig. 2. Single bubble; (a) flow domain with initial vapour fraction; (b) generated grid with initial pressure distribution. (For interpretation of the references to colour in this figure legend, the reader is referred to the web version of this article.)

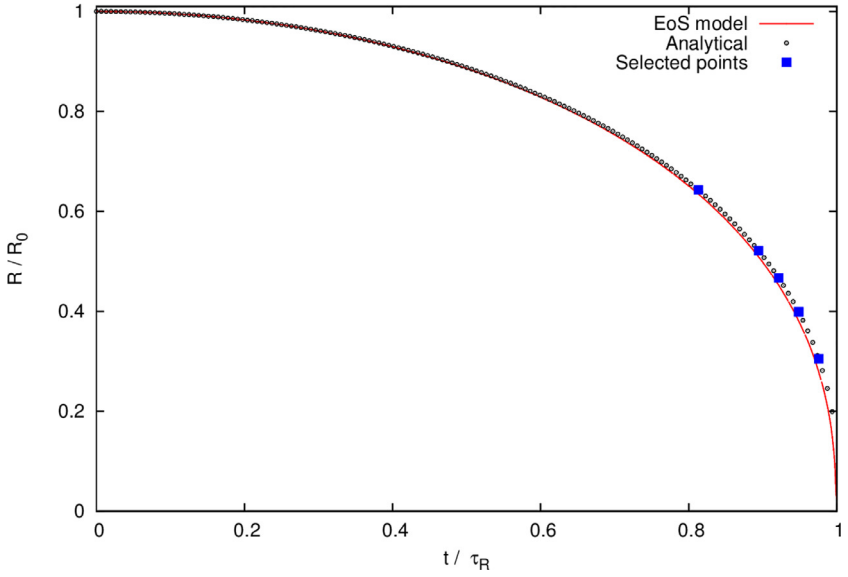

Fig. 3. Validation of the equilibrium (EoS) model in predicting the evolution of the bubble radius.

equivalent radius of the total vapour volume. As depicted in the figure, the radius profile is well captured by this method.

In Fig. 4, the pressure distribution in the radial direction is compared with the analytical data at different normalized time steps. In this figure, the normalized times t/τ_R of 0.812, 0.894, 0.921, 0.948 and 0.975 are chosen which are corresponding to non-dimensional radius (R/R_0) values of 0.64, 0.52, 0.47, 0.4 and 0.3, respectively. The selected instances are shown in Fig. 3 as well. At these steps, the bubble size variation is quite fast and the surrounding flow field changes rapidly. Before $t/\tau_R = 0.812$, the pressure variations around the bubble does not have large gradients and the profile is rather similar to the initial distribution. Considering the stated assumptions, the pressure is expected to be equal to the vapour pressure inside the bubble, which corresponds to a non-dimensional value of -1. From the bubble interface to the farfield, the pressure increases to the farfield pressure. However, according to Eq. (28), its profile has a maximum value close to the interface if $R/R_0 < 0.63$ (Franc and Michel, 2006). This behaviour is clearly seen from the analytical solution in Fig. 4a. The numerical results also follow the general trend, but with some noticeable differences. First, the pressure near the interface is still close to vapour pressure and the pressure increase starting point seems to be at a radius larger than the bubble radius. This inconsistency can be due to the numerical diffusivity of the bubble interface, shown in Fig. 5. In this figure, an imaginary red line shows the exact bubble radius overlayed on predicted vapour fraction and pressure fields at $t/\tau_R = 0.812$. In Fig. 5a, the computed vapour fraction distribution over the discretized domain is shown. It is seen that the bubble interface is diffused over three layers of radial cells (the orange, the green and the light blue cells), which means that in these cells the fluid is considered as a saturated mixture in the equilibrium model and the pressure, in the last layer (outside exact bubble radius) cannot vary considerably from the vapour pressure. In Fig. 5b, the pressure contour around the bubble is depicted. It is seen in this figure that the pressure is equal or close to the vapour pressure up to one cell layer after the bubble radius. Since the radial edge size of each cell is 0.02 mm (initial radius is resolved by 20 radial cells) this discrepancy is comparable to what is shown in Fig. 4a. In Fig. 5c the same contour is plotted with local scale (i.e. $2,320 < p < 2,380$ Pa) and it shows that inside the bubble

Please cite this article as: E. Ghahramani et al., A comparative study between numerical methods in simulation of cavitating bubbles, International Journal of Multiphase Flow (2018), https://doi.org/10.1016/j.ijmultiphaseflow.2018.10.010

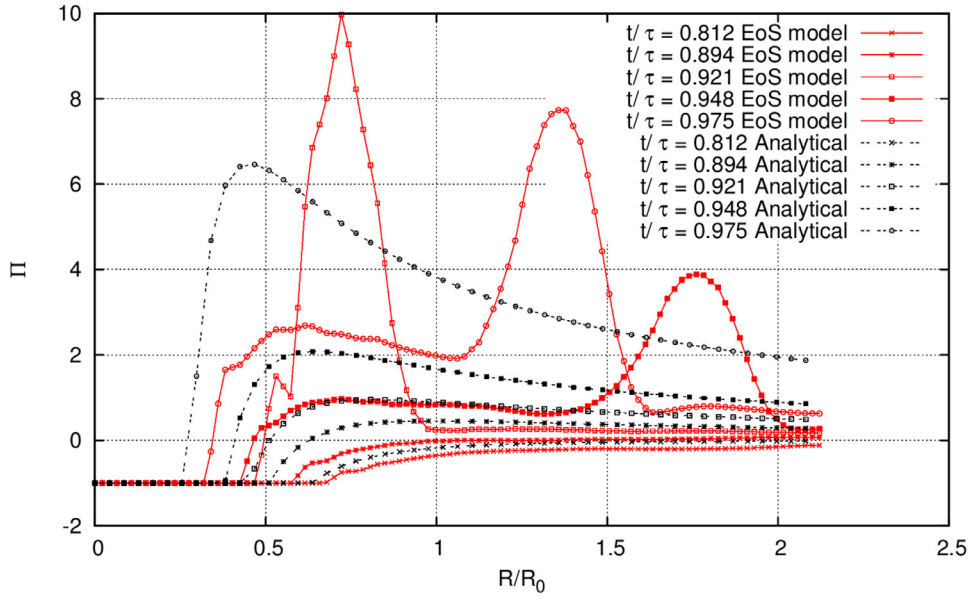

(a)

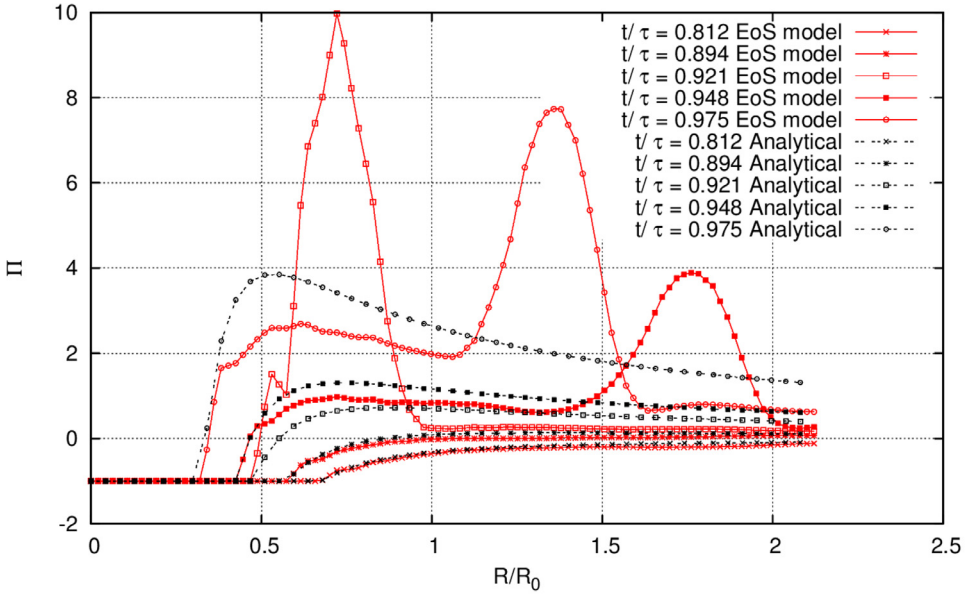

(b)

Fig. 4. Comparison of equilibrium (EoS) model pressure distribution with analytical data; (a) at similar radius; (b) at shifted interface.

the pressure is not exactly estimated as constant, especially in four radial layers where the fluid is saturated mixture, c.f. Fig. 5a. In these layers, the temperature has a small variation (less than 0.5 degrees) and it causes around 40 Pa variation in the saturated pressure value. This is one of the capabilities of the temperature dependent equations of states that consider the temperature changes during cavitation.

To have a better understanding of the model performance in calculation of pressure field outside the bubble, the analytical data are shifted a little in Fig. 4b. In fact, in the new analytical profiles, the sharp bubble interface is assumed to be equal to the outer edge of the diffused numerical interface so that both pressure profiles have similar gradient at the interface. From this figure it can be inferred that the equilibrium model would be capable to predict outer pressure profile more reasonably if the interface could be captured sharply and at the correct location. However, the pressure is still a little underestimated at the later steps, i.e $t/\tau_R = 0.948$ and 0.975. Besides that, some large wiggles are seen in the pressure profile which are due to numerical pressure waves that are emitted from bubble interface. When the fluid phase changes from vapour to liquid in a computational cell, there is a change in the relative equation of the state for the fluid and the general profile of the density-pressure relation changes. Such a change in the modelling equations causes some spurious pulse in the flow. Since in the polar grid that is aligned with the interface, phase change occurs in all cells of a radial layer simultaneously, the numerical pulses of the neighbouring cells are superposed and generate a significant disturbance. In a Cartesian grid, for example, the vapour collapse at neighbouring cells does not happen simultaneously and the wiggles in the pressure profile are expected to cancel and be

Please cite this article as: E. Ghahramani et al., A comparative study between numerical methods in simulation of cavitating bubbles, International Journal of Multiphase Flow (2018), https://doi.org/10.1016/j.ijmultiphaseflow.2018.10.010

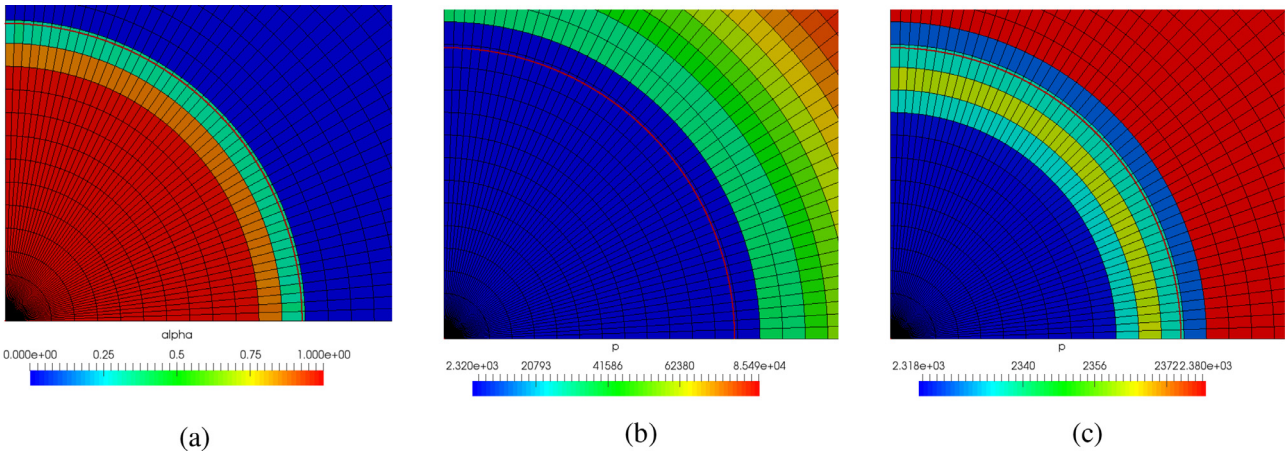

Fig. 5. Resolution of bubble interface from the equilibrium model at $t/\tau_R = 0.812$; (a) vapour volume fraction contour; (b) pressure contour at global scale; (c) pressure contour at local scale. The red line depicts the bubble radius of the analytical solution. (For interpretation of the references to colour in this figure legend, the reader is referred to the web version of this article.)

smaller; this is observed in the second case of the bubble cluster. Furthermore, these pulses are a function of numerical discretization schemes as well and more diffuse schemes are expected to generate smaller pulses.

To investigate the effect of the grid resolution on the model results, the problem is solved with a coarser grid in which the initial bubble is discretized with 12 cells (i.e. $\Delta_r/R_0 = 0.083$). In Fig. 6, the estimated bubble radius and pressure profiles are compared with the corresponding ones of the fine grid. For the bubble radius, the results are very similar, however, considerable differences are seen for the pressure estimation. For the coarse grid, the maximum non-dimensional pressure peak is 32, which is not seen in the plot range.

3.2. Finite mass transfer model result

The temporal evolution of bubble radius for the finite mass transfer model is compared with the exact analytical solution in Fig. 7. According to this figure, the finite mass transfer model is capable in estimation of bubble radius profile if the empirical coefficients are set high enough. In fact, with low coefficients values, the bubble collapses very slowly.

To have a better understanding of the model performance in resolving the flow field, the collapse pressure profiles are compared with analytical data in Fig. 8. It is seen that although moderate coefficient values ($C = 100$) can capture the radius evolution, there may be numerical issues in representing the pressure field. In Fig. 8a, it is seen that in the last stages of collapse ($t/\tau_R > 0.921$), the pressure inside the bubble is overestimated. Besides that, some numerical pulses are created at the interface which cause the outside pressure at $t/\tau_R = 0.921$ to be higher than the corresponding value at $t/\tau_R = 0.948$, for example. Here, ignoring the pure phase compressibility is also affecting the prediction. As seen in the compressible equilibrium model results (Fig. 4), a numerical pulse causes a pressure wave that is emitted gradually in the domain and therefore, (only) the local pressure is increased. However, for the finite mass transfer model in this study, the liquid is assumed to be incompressible and a local numerical pulse increases the whole domain pressure instantaneously. Therefore, the outside pressure profile at $t/\tau_R = 0.921$ is higher than the corresponding profile at $t/\tau_R = 0.948$. Further increasing the coefficient to 500 or 1000 solve the inside pressure overestimation issue, however, the numerical pulses get more significant. If the coefficients are increased to 10^4, then both of the issues are approximately addressed. However, similar to the equilibrium model, the interface is diffused and the pressure increase starting point is shifted a little in the radial direction and the pressure peaks are underestimated. If the coefficients are increased to very high values (Fig. 8c) the pressure profile does not change considerably. However, comparison of profiles at $t/\tau_R = 0.921$ and 0.894 shows that small numerical pulses still appear in the simulation. It should be mentioned that increasing the model constants may decrease the stability of the problem and special measures should be done to make sure a converged solution of the vapour transport equation is achieved. The general trend of pressure profile relative to the model constants are in agreement with the work of Schenke and van Terwisga (2017) in which they used the Merkle mass transfer model (Merkle et al., 1998) and concluded that for more satisfactory resolution of bubble Rayleigh collapse, the model constants should be quite large while the time steps should be fine enough.

Another parameter that can be effective on model performance is the time step size. In this study, the very small time step of $dt = 5 \times 10^{-9}$ s was chosen at first, to make sure that it works for different applied models. This value may work for EoS model as well, but to avoid some pressure fluctuations and to satisfy the CFL number limitation, a smaller time step was used in the compressible approach. For the FMT model, however, a time step study of the finite mass transfer model (Fig. 9) shows that the time step should be smaller than 5×10^{-8} s to ensure time-step independent solution. Further time step study (not reported here) confirms converged solution using $dt = 5 \times 10^{-9}$ s. However, smaller time steps may increase the solution instability, and the solution parameters need to be set more carefully, e.g. by decreasing the solution tolerances or setting a minimum number of iterations, to ensure converged result for high values of mass transfer coefficients. Also, from Fig. 9 it seems that the spurious numerical pulses may be avoided by increasing the simulation time step; however, it can be shown that there is not a predictable relation between these pulses and the time step, as for time steps larger than 5×10^{-8} s (e.g. 1×10^{-7} s), some spurious pulses are seen in the domain that are larger than the previous ones.

To investigate the model dependency on the grid resolution, the problem is solved with a coarser grid ($\Delta_r/R_0 = 0.083$) as well. In Fig. 10, the estimated bubble radius and pressure profiles with empirical coefficients of 10^4 are compared with the corresponding ones of the fine grid. It is seen that while the bubble radius is well estimated with the coarser grid, considerable numerical pulses appear in the solution even with the high mass transfer coefficients. This is an important point, since in typical engineering problems, the small cavity structures are not discretized with very fine grids.

Please cite this article as: E. Ghahramani et al., A comparative study between numerical methods in simulation of cavitating bubbles, International Journal of Multiphase Flow (2018), https://doi.org/10.1016/j.ijmultiphaseflow.2018.10.010

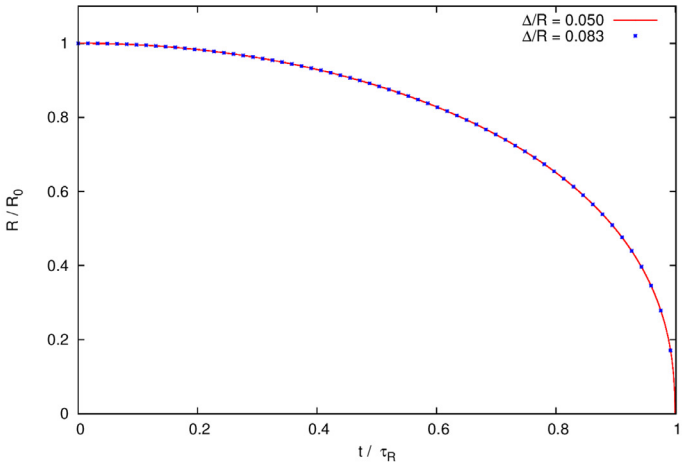

(a)

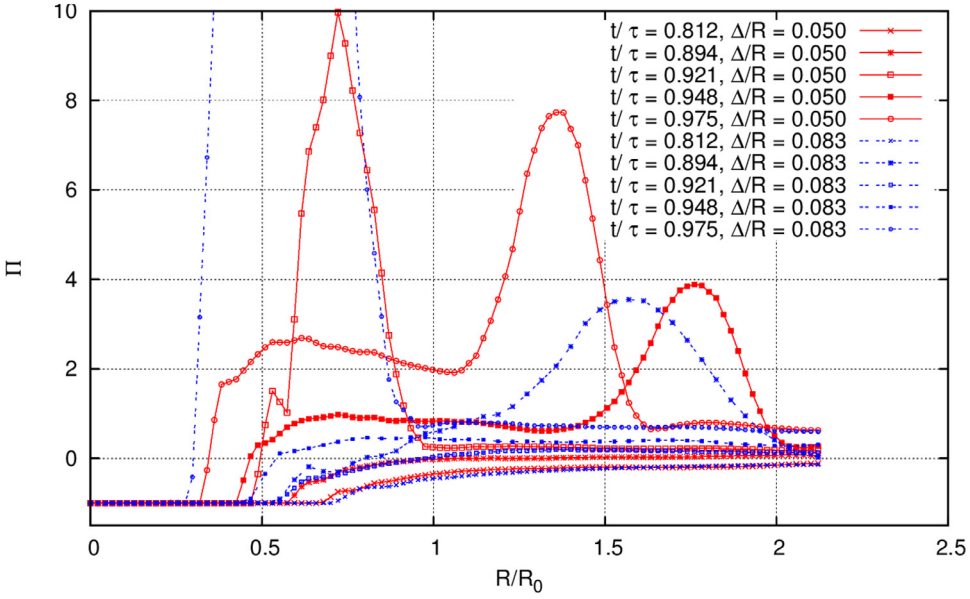

(b)

Fig. 6. Domain discretization effect on the equilibrium model; (a) bubble radius; (b) pressure profile.

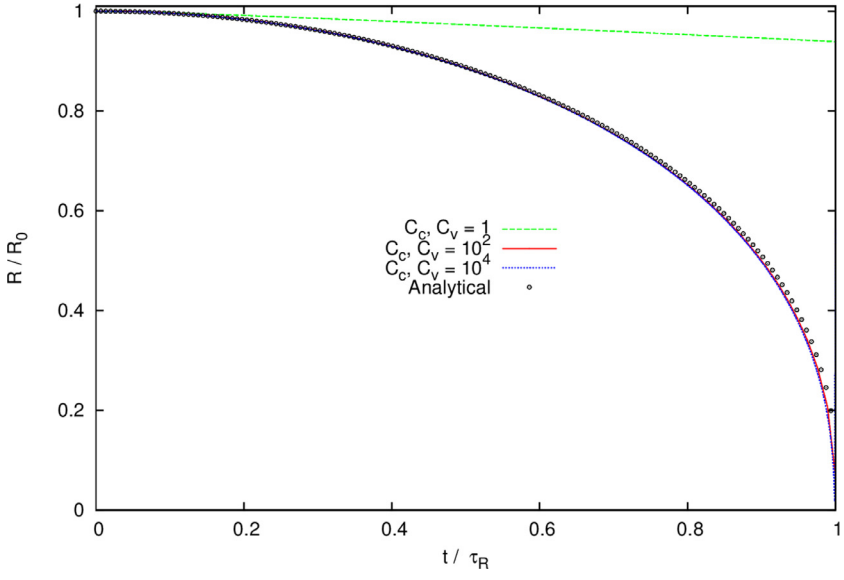

Fig. 7. Validation of the finite mass transfer model with different coefficients in predicting the evolution of the bubble radius.

Please cite this article as: E. Ghahramani et al., A comparative study between numerical methods in simulation of cavitating bubbles, International Journal of Multiphase Flow (2018), https://doi.org/10.1016/j.ijmultiphaseflow.2018.10.010

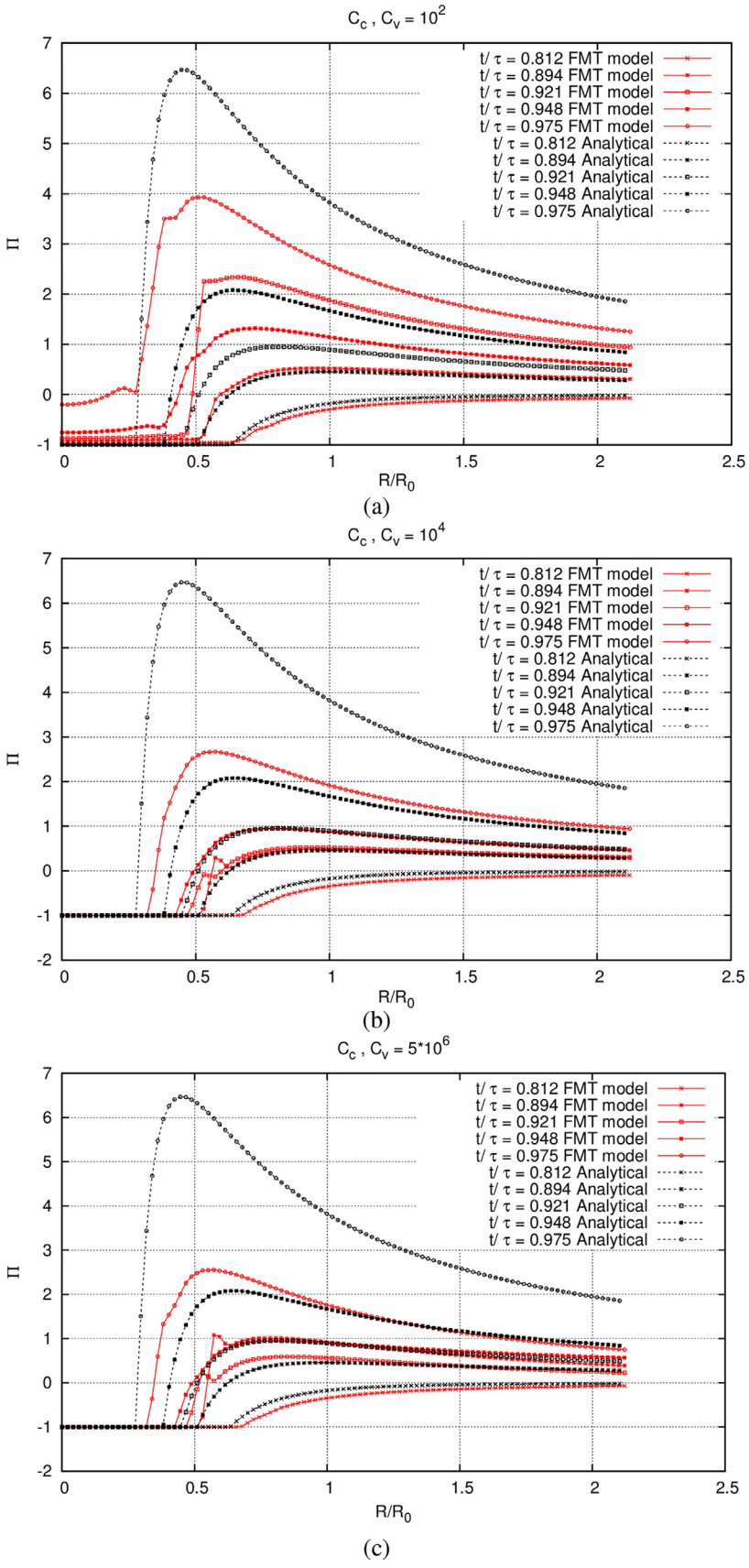

Fig. 8. Comparison of finite mass transfer (FMT) model pressure distribution with analytical data; (a) $C_c = C_v = 10^2$; (b) $C_c = C_v = 10^4$; (c) $C_c = C_v = 5 \times 10^6$.

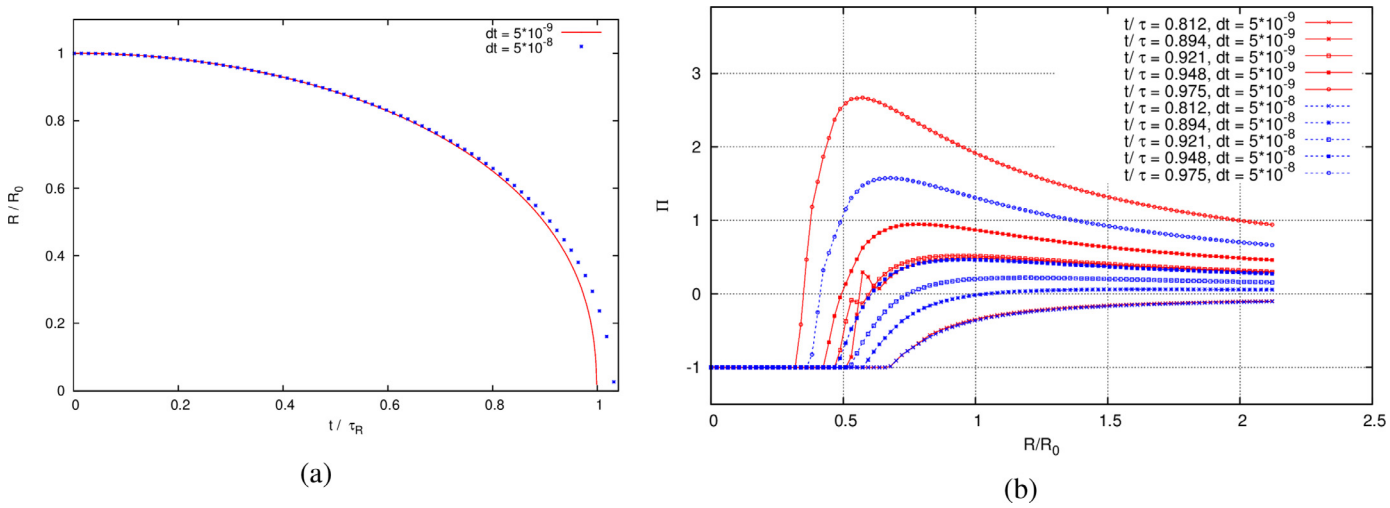

Fig. 9. Time-step dependency of the finite mass transfer model; (a) bubble radius; (b) pressure profile.

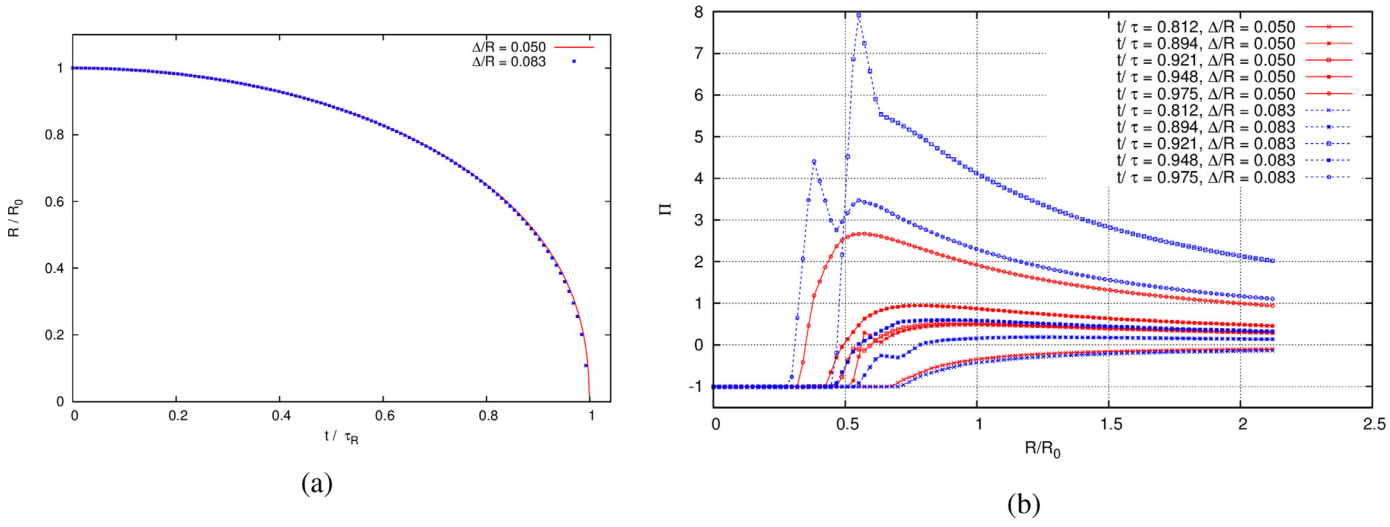

Fig. 10. Domain discretization effect on the finite mass transfer model; (a) bubble radius; (b) pressure profile.

3.3. Lagrangian model result

In the Lagrangian model, the governing equations are similar to those of finite mass transfer model and only the bubble dynamics are resolved by solving the Rayleigh–Plesset (R–P) equation, instead of solving the Eulerian vapour transport equation. Therefore, the numerical schemes are similar to those of the previous section. In this section, first the Lagrangian results based on the original form of the R–P equation are presented. In the original form of the equation, the farfield pressure is known and constant. Since we have the exact profile of bubble radius in such case, the vapour fraction field is resolved accurately and the result can be used to investigate the pressure equation and mass transfer rate. The problem is also solved based on the localized form of R–P equation (Eq. (25)) to investigate the effect of local pressure in calculation of bubble dynamics since the original form of R-P is not applicable in more complicated problems, as will be shown later.

In Fig. 11, the obtained pressure profile from the Lagrangian approach with original R-P is compared with the analytical data for two different mass transfer coefficients. Similar to the Eulerian model, the coefficients should be high enough for an accurate estimation of pressure inside the bubble; however, even with small coefficients no numerical pulse is seen in the Lagrangian model results and the outside pressure profiles are very well estimated, Fig. 11a. Also, for this model, one only needs to make sure that the coefficients are high enough and the pressure profile are well captured even at the last stages of collapse, Fig. 11b. It should be mentioned that the solution instability problems, that were mentioned for the finite mass transfer model above, do not exist for this Eulerian–Lagrangian approach, even when increasing the model constants to very high values or decreasing the time step to smaller ones. It seems that for the bubble Rayleigh collapse with the stated assumptions, the issue with the finite mass transfer model is related to the scalar transport equation of vapour fraction. When the exact value of bubble radius is known at each time step and the interface is sharply captured, the pressure equation (continuity) is solved accurately and only the mass transfer rate should be high enough to compensate for the bubble inertia in the Rayleigh–Plesset equation that was simplified in finite mass transfer models.

The inherent issues with the original form of Rayleigh–Plesset equation are its dependency on the constant known farfield pressure and the assumption of unrestricted field around the bubble. In most practical applications, the bubble is surrounded by other cavity structures and local flow effects need to be considered. There are modified versions of the equation in literature in which the local flow pressure on the bubble interface, or near that, is used in the equation (instead of p_∞) and to compensate for

Please cite this article as: E. Ghahramani et al., A comparative study between numerical methods in simulation of cavitating bubbles, International Journal of Multiphase Flow (2018), https://doi.org/10.1016/j.ijmultiphaseflow.2018.10.010

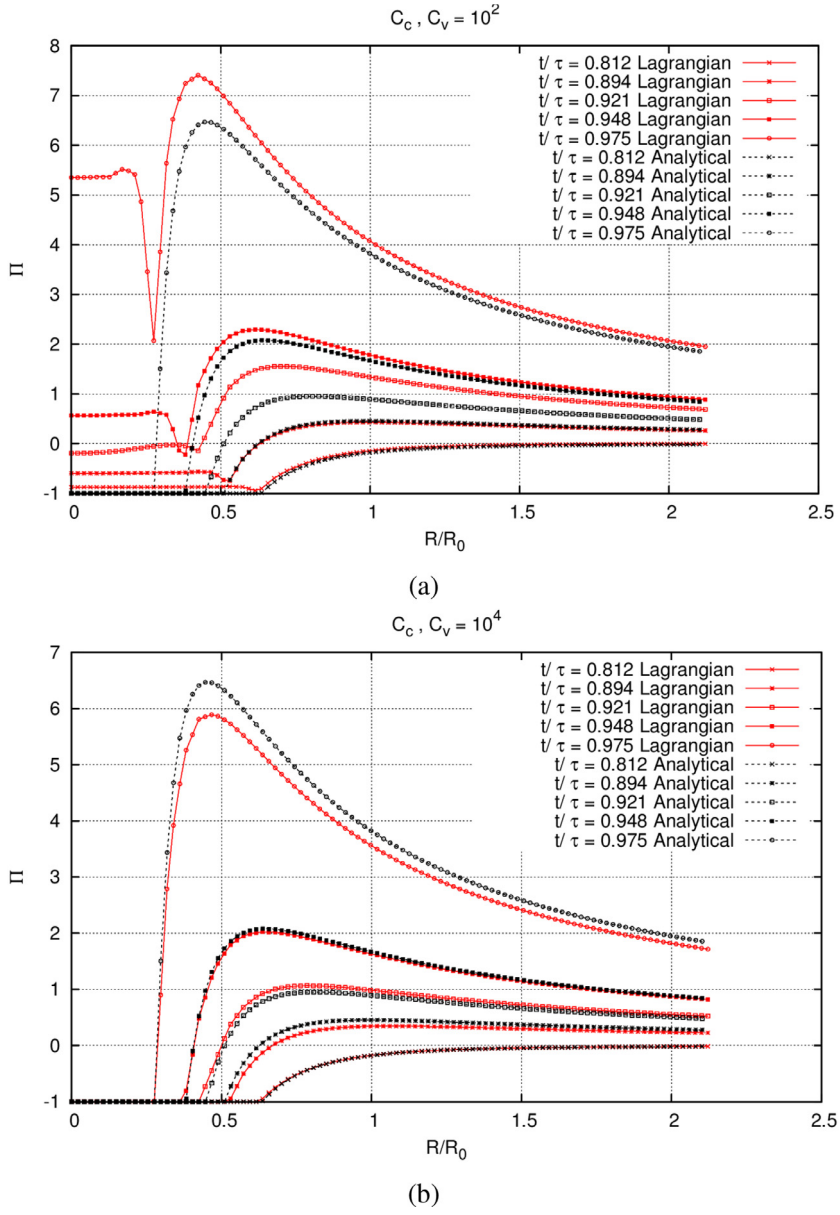

Fig. 11. Comparison of Lagrangian model based on original R–P equation with analytical data in calculation of pressure distribution; (a) $C_c = C_v = 10^2$; (b) $C_c = C_v = 10^4$.

this simplification some correction terms are added to the equation. For example, Hsiao et al. (2000) suggested a slip velocity correction term based on the bubble-flow velocity difference. Also, Giannadakis (2005) proposed another correction term based on local turbulence quantities. However, for this simple collapse problem, such modifications in the equation cannot improve the results as the flow velocity is very small and there is no turbulence in the symmetrical flow around the bubble. As a solution, the equation was re-derived here based on the local pressure value as stated before, using Eq. (25).

In Fig. 12, the Lagrangian model performance based on the localized R–P equation is validated with the analytical solution. Here, only the high coefficient ($C = 10,000$) result is presented, as the lower coefficients were shown to be problematic in pressure estimation inside the bubble, as discussed above. It is seen that the bubble radius evolution is well captured with the localized R-P as well. In Fig. 13, the pressure lines for different time steps are compared with analytical solution which shows that this model can estimate the pressure peaks and their location with good accuracy

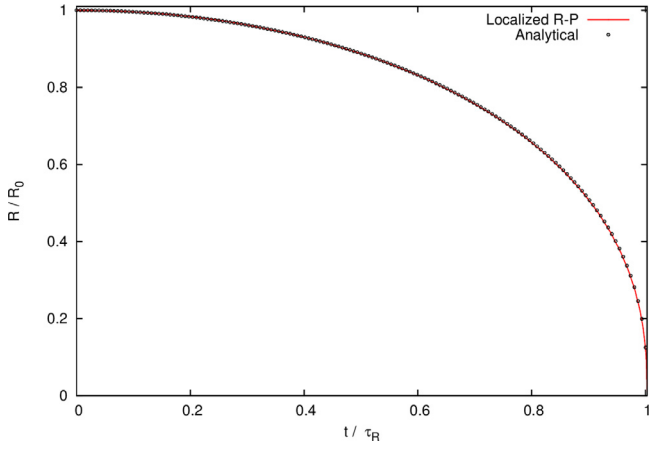

Fig. 12. Validation of Lagrangian model based on localized R–P equation in predicting the evolution of the bubble radius.

Please cite this article as: E. Ghahramani et al., A comparative study between numerical methods in simulation of cavitating bubbles, International Journal of Multiphase Flow (2018), https://doi.org/10.1016/j.ijmultiphaseflow.2018.10.010

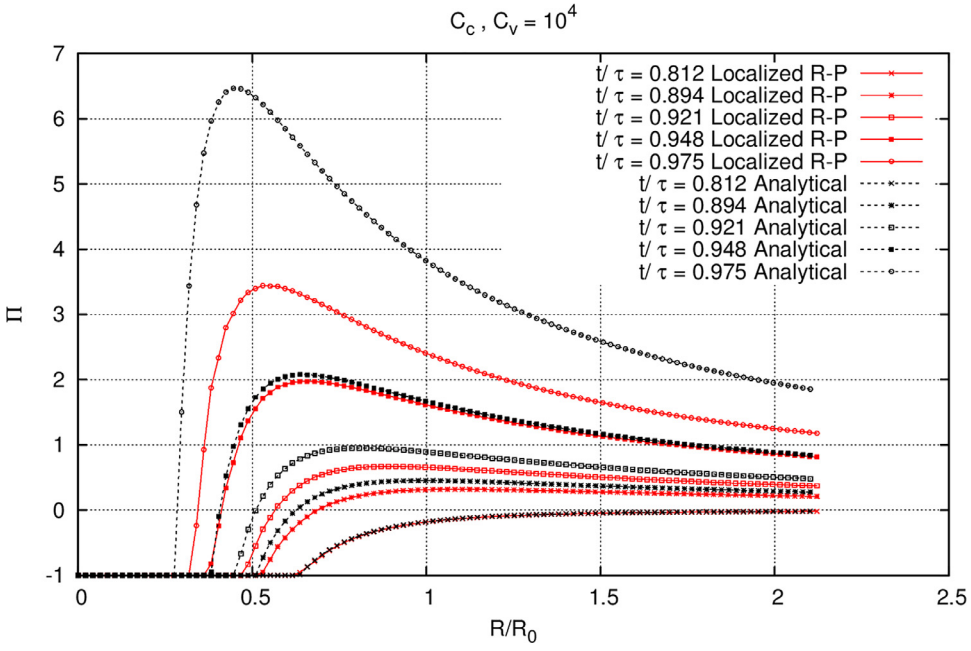

Fig. 13. Comparison of Lagrangian model based on localized R–P equation with analytical data.

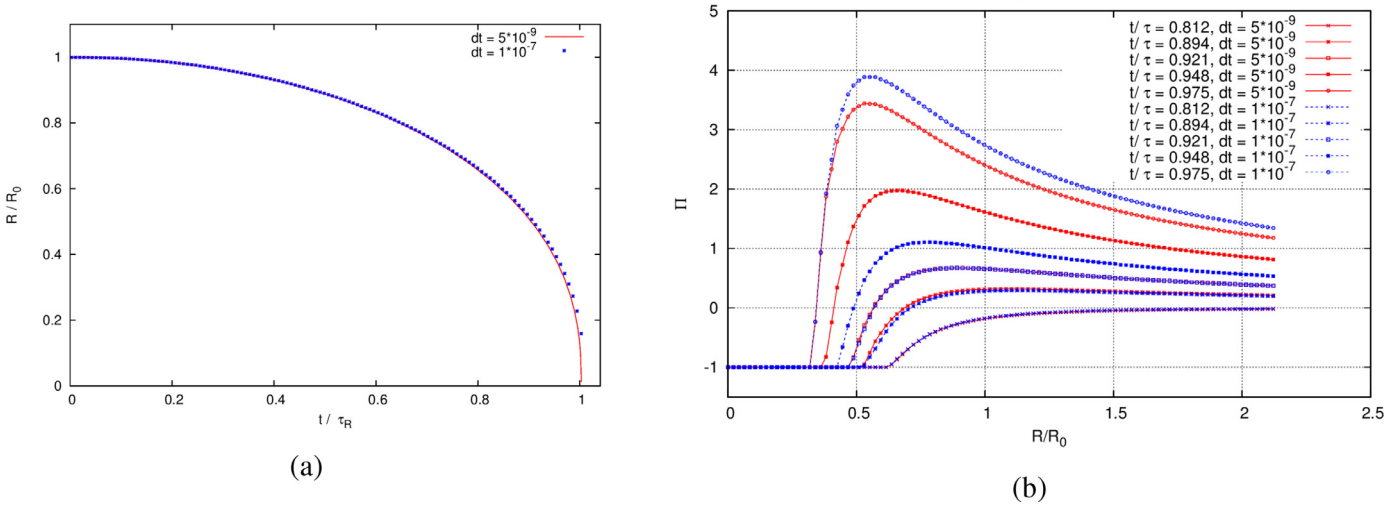

Fig. 14. Time-step dependency of the Lagrangian model based on localized R–P equation; (a) bubble radius; (b) pressure profile.

and without any numerical pulse or significant delay in the pressure increase starting point. Only after $t/\tau_R > 0.95$ some discrepancy is seen between numerical and analytical data and it is due to the localized R–P equation dependency on the exact estimation of local pressure. During the last stages of the collapse, the pressure field around the bubble varies quite rapidly and a small error in pressure estimation can lead to considerable difference in bubble radius calculation which leads to more discrepancy in the following time steps. However, the estimated pressure in the last steps is still acceptable as compared to finite mass transfer and equilibrium models results.

In Fig. 14, the results using a larger time step, $dt = 1 \times 10^{-7}$ s, are compared to the obtained data with $dt = 5 \times 10^{-9}$ s). The results are overall similar for bubble radius as well as pressure profiles and only in one time step ($t/\tau_R = 0.948$) the pressure line has a small shift.

To study the model dependency on the grid resolution, the problem is solved with a coarser grid ($\Delta_r/R_0 = 0.083$) as well. In Fig. 15, the calculated bubble radius and pressure profiles with empirical coefficients of 10^4 are compared with the corresponding ones of the fine grid and it is seen that even with coarser spatial discretization, the model has an acceptable accuracy and no numerical pulse is generated in the domain. It can be concluded that the Eulerian–Lagrangian model can produce satisfactory results with larger time steps and coarser grids as compared to other models.

It should be mentioned that for the local form of the R–P equation, other radial distances for local pressure value have been tested as well, and the pressure profile has similar trend and only the quantitative difference with the theoretical profile varies a little for different radial distances; smaller distances (such as r = 2R) leads to a little more accuracy.

Please cite this article as: E. Ghahramani et al., A comparative study between numerical methods in simulation of cavitating bubbles, International Journal of Multiphase Flow (2018), https://doi.org/10.1016/j.ijmultiphaseflow.2018.10.010

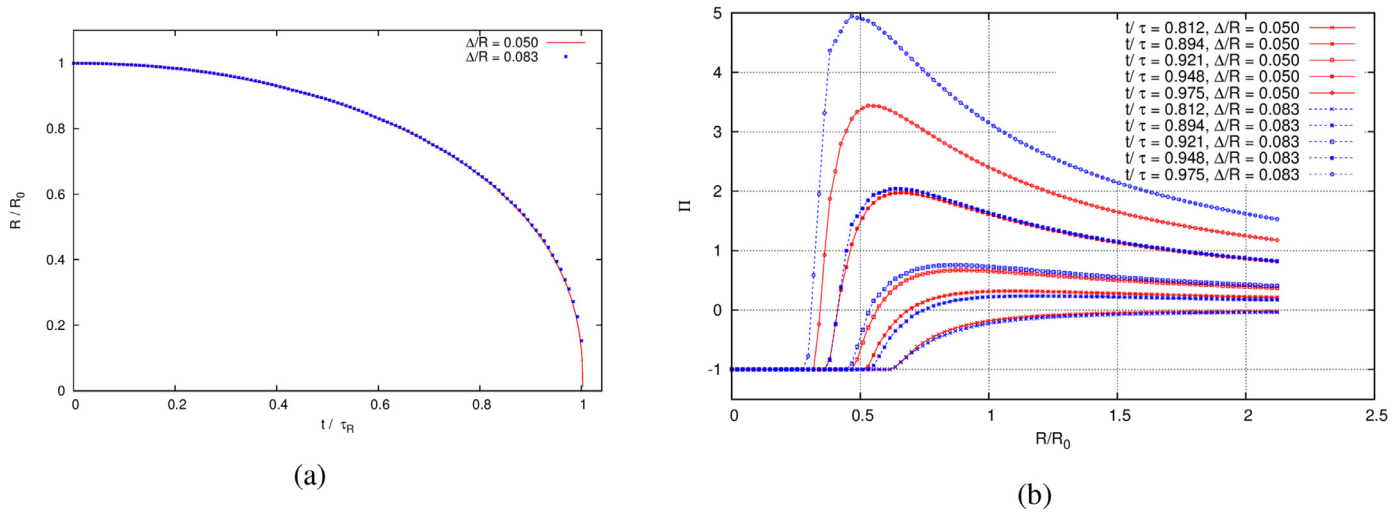

Fig. 15. Domain discretization effect on the Lagrangian model based on localized R–P equation; (a) bubble radius; (b) pressure profile.

The single bubble collapse is a simple problem that can clarify the basic behaviour of the numerical approaches. However, the bubbles are usually surrounded by other cavity structures and the flow field can be restricted by wall boundaries. Also, there are special cases where the ambient pressure is such high that the observed numerical pulses are of minor importance and we are more interested in measuring large collapse pressures. In the following part, a more complex test case is simulated to analyse the models behaviour regarding these effects.

4. Collapse of a bubble cluster

In this section the collapse of a cluster of bubbles over a flat wall is simulated. Here, the bubble dynamics is affected by the collapse of the surrounding bubbles as well as the near wall influence. In the current study, the bubble cloud which was previously defined by Schmidt et al. (2011) is used. This cloud consists of 125 spherical vapour bubbles with a radius distribution ranging from 0.70 mm to 1.64 mm with non-uniform distribution. The average radius of the bubbles is 0.95 mm and they have a minimum distance of 0.2 mm to avoid intersection. Also, they have larger concentration and radii around the centre of the cloud. The overall cloud is located in a small liquid-filled cubic domain of $20 \times 20 \times 20$ mm^3 and has a total volume fraction of 5.8%. The cubic domain, itself, is located in a larger rectangular domain of $4 \times 4 \times 2$ m^3 and the bottom faces of the two domains are coplanar. The bubble distribution inside the inner domain is depicted in Fig. 16. Recently, Ogloblina et al. (2017) investigated the bubble-bubble interaction and the stand-off distance effects on the collapse behaviour of the cluster and based on the obtained results, it can be concluded that the bubble interactions in the currently used cluster are significant.

The fluid domain is assumed to have a stationary initial condition with a uniform temperature of 293 K. The initial pressure inside the bubbles is set equal to the vapour pressure of 2,340 Pa and in the surrounding liquid it is assumed to have a Laplacian distribution, which is reasonable for a stationary condition. The coplanar bottom faces of the domain are defined as impermeable walls and other outer faces are considered as far-field boundaries with constant pressure of 40 bar and no gradient of other flow parameters.

To discretize the bubble cloud, the small domain consists of 55^3 Cartesian structured cells with the numerical resolutions (Δ_{CFD}) of 0.36 mm, and it is equivalent to Grid 3 in the work of Schmidt et al. (2014, 2011). In this discretization, the smallest bubbles are represented by about 32 cells and the largest ones are discretized by more than 400 cells, which approximately corresponds to $0.2 < \Delta/R < 0.5$; it is thus coarse compared with the resolutions studied for the single bubble collapse. In Fig. 17 the contours of the initial solution are shown. The vertical cut planes are vapour fraction fields in the small inner domain using cell values (right) and continuous colouring (left), while the bottom horizontal face depicts the pressure field on the bottom face of the inner domain. In this figure, the upper limit of vapour fraction contours is set to 0.5 for better contrast. The time step of the simulations is 3.9×10^{-8} s corresponding to CFL number (for compressible solution) of 0.7 and the sampling frequency of 2.56×10^7 Hz. Finally, in order to measure the imposed pressure of the collapsing bubbles on the bottom wall, one pressure transducer is located at the centre of the bottom face. This transducer covers an area of 1×1 cm^2.

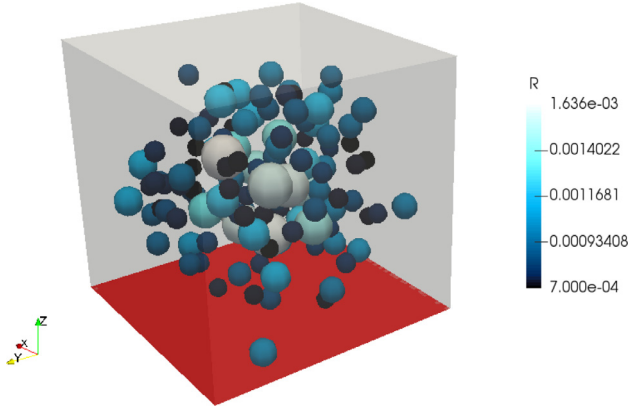

Fig. 16. Distribution of 125 spherical non-intersecting bubbles within the small cubic domain of 20^3 mm^3 over a flat wall (red surface). This small domain is inside a larger outer domain of $4 \times 4 \times 2$ m^3 (not shown here). (For interpretation of the references to colour in this figure legend, the reader is referred to the web version of this article.)

To validate the simulations, first the equilibrium model results are compared with the data of Schmidt et al. (2014, 2011). In Fig. 18a, the dimensionless volume variations of the bubble cloud and collapse durations are compared. As there is no experimental data or analytical solution for this specific cloud with the specified boundary conditions, a simplified analytical estimation is utilized to evaluate the general trend of the results. Assume the col-

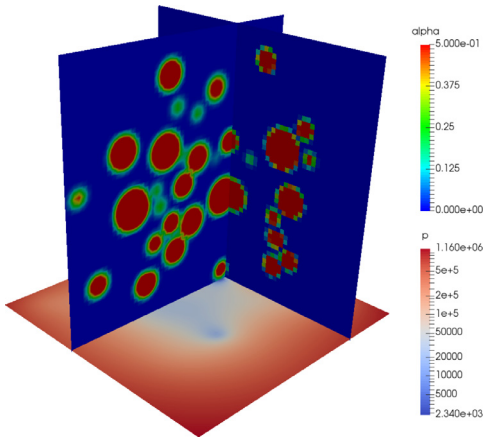

Fig. 17. Initial flow contours: vapour fraction using cell values (vertical right); vapour fraction using point values for continuous colouring (vertical left); pressure (horizontal). (For interpretation of the references to colour in this figure legend, the reader is referred to the web version of this article.)

lapse of an *equivalent bubble* with the same initial vapour volume as the bubble cloud, yielding an initial equivalent radius of 4.8 mm. The Rayleigh collapse time of this bubble in a farfield pressure of 40 bar is 6.9×10^{-5} s (Eq. (26)). The collapse time of the numerical cloud in the current simulation is 7.3×10^{-5} s while from the work of Schmidt et al. (2014) it is found to be 6.3×10^{-5} s. Therefore, both estimated collapse times are reasonable. The volume variation profile of the equivalent bubble is also plotted in Fig. 18a for comparison. From the collapse time and volume variation profiles it is seen that there is a time shift between the two simulations. This shift is seen in the pressure profile as well, see Fig. 18b. This is probably due to an anticipated small difference between the initial pressure field of the two simulations. However, the profiles look very similar for both volume variation and wall pressure, and after the initial shift the simulation profiles are almost parallel. There is also some difference in pressure peak values which is due to different flux schemes that were used in the simulations. In the pressure profile, the result of a finer grid ($\Delta_{CFD} = 0.09$ mm) is shown as well and it is seen that the results of the current study is more similar to the fine grid profile of Schmidt et al. (2014).

In Fig. 19, the vapour volume variations of the finite mass transfer model with different mass transfer coefficients are compared to the equilibrium model result. It is seen that with different mass transfer coefficients, the finite mass transfer model estimate similar variation for the total volume of the cloud with time. For the single bubble collapse, it was found that when the empirical constants are larger than a minimum value, the bubble radius profile does not show a considerable change. For a cloud of bubbles with a large ambient pressure (40 bar in this case), however, the total volume of the cloud does not change significantly with the chosen range of coefficient values, although individual bubbles may have different radius variations which can be anticipated from small differences between $C = 1$ profile and the others.

The temporal evolution of cloud volume for the Lagrangian model based on different R–P equations are compared to the equilibrium model in Fig. 20. Three different forms of the R–P equation are used in these simulations. The first one is the original form of the equation (Eq. (24)) with the infinity pressure (p_∞) value equal to the pressure at the farfield boundaries (40 bar). The other case is the original form in which the liquid surface average pressure at the bubble interface is used as p_∞. As stated before, this approach has been used in literature as a simplified method to consider local flow effect on the bubble. The third case is the localized R–P equation (Eq. (25)). It is seen in the figure that the original R–P equation with farfield pressure estimates a faster collapse. This is expected since the farfield pressure (40 bar) is much larger than the effective local pressure around the bubble. Also, replacing the farfield pressure with the corresponding value at the interface leads to a very slow rate of collapse and after 70 μs only 15 percent of the cloud volume is condensed. In previous studies, this approach has been modified by correction terms such as a constant pressure added to p_∞, slip velocity correction term (Hsiao et al., 2000) or corrections based on the turbulence quantities (Giannadakis, 2005). However, such corrections do not work for this problem, since the slip velocity and the turbulence level are negligible and the corrected constant pressure is unknown. Comparing to these two forms, the localized R–P equation can capture the collapse rate very well. In fact, the estimated collapse time is close to the one from equilibrium model and the total volume profile is very similar to the finite mass transfer method result, see Fig. 19. It should be mentioned that for the localized R–P equation, the empirical constants should be larger than a minimum value ($C \approx 100$) to capture the volume profile reasonably. It is shown later that with smaller coefficients, the pressure field is not well-estimated and it affects individual bubble collapse in the Lagrangian approach. However, after this minimum value, the cloud rate of collapse is independent of the mass transfer coefficients.

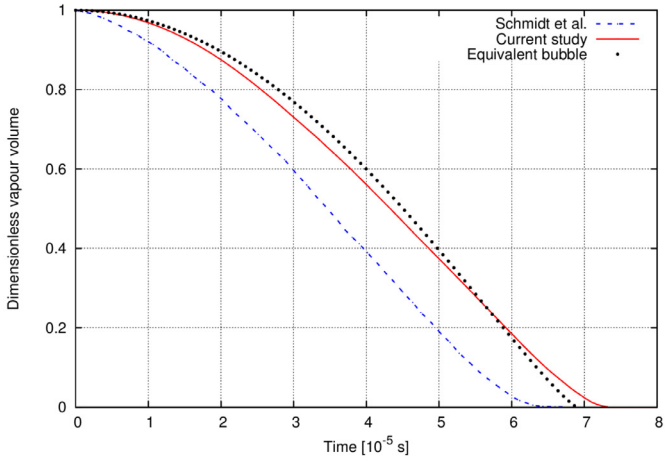

(a)

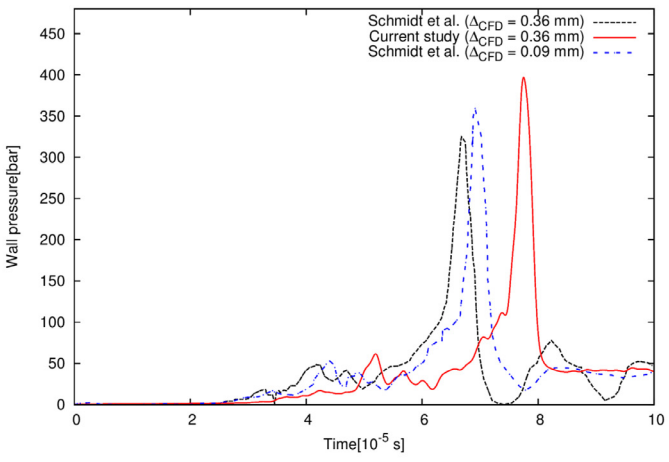

(b)

Fig. 18. Validation of the equilibrium model simulation of bubble cluster; (a) time history of the vapour volume; (b) average pressure on the wall transducer.

Please cite this article as: E. Ghahramani et al., A comparative study between numerical methods in simulation of cavitating bubbles, International Journal of Multiphase Flow (2018), https://doi.org/10.1016/j.ijmultiphaseflow.2018.10.010

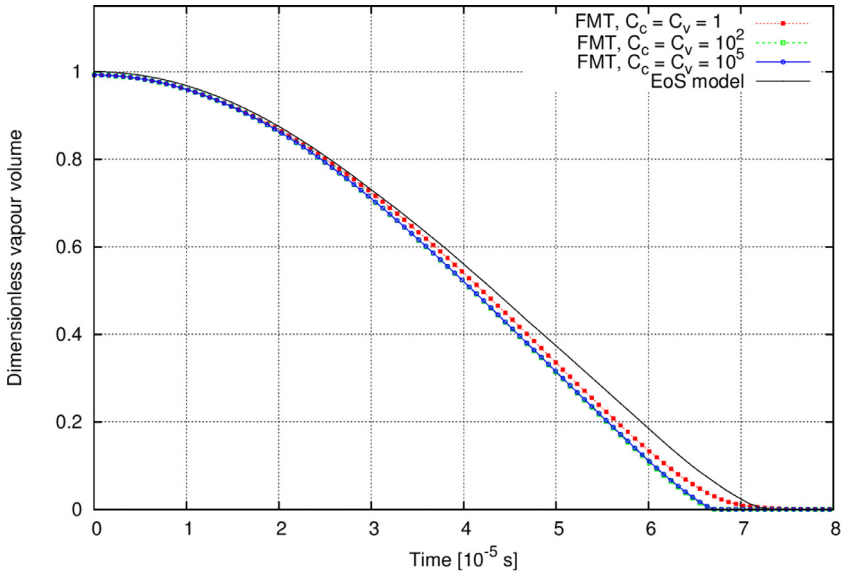

Fig. 19. Time history of bubble cloud volume using finite mass transfer model (FMT) with different coefficients.

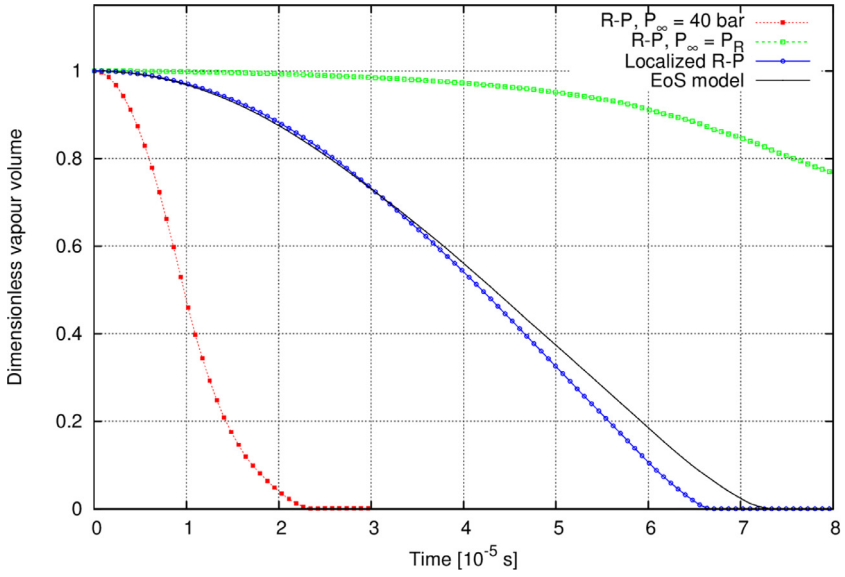

Fig. 20. Time history of bubble cloud volume using Lagrangian model with different R–P equations.

In Fig. 21, the average pressure profiles of the finite mass transfer model on the 1×1 cm^2 pressure transducer are compared with the equilibrium model result. For the single bubble collapse some numerical wiggles were detected in the pressure profiles of the equilibrium model results and as stated, in the polar grid, due to the simultaneous phase change in several polar cells (equidistant to the centre), these wiggles are augmented and form larger pulses. In the bubble cluster case, however, a Cartesian grid is used and the numerical pulses are negligible compared to large physical collapse pressure peaks. In fact, no considerable numerical pulse is seen in the average pressure profile over the small transducer (Fig. 18b) and the local peaks of the equilibrium model profile are related to the collapses of different bubbles. Therefore, the equilibrium model result can be considered a reasonable benchmark solution for estimation of the finite mass transfer model performance. In Fig. 21a, it is seen that the pressure estimation of the finite mass transfer model is highly dependent on the empirical coefficients, contrary to what was noted for the volume variation. If the coefficients are low, no local pressure peak is seen from individual bubble collapse and the average pressure on the wall increases smoothly to the maximum value which corresponds to the final violent collapse, and after the collapse it decreases smoothly. When the coefficients are increased to moderate values ($C = 10^2$), there are some local peaks in the wall pressure profile and the maximum pressure value is estimated much larger than the corresponding value of compressible equilibrium model. When the coefficients are further increased to high values ($C = 10^5$), these peaks still exist and it is seen that for both moderate and high coefficients they are so frequent that the profile is not a regular line. It should be mentioned that the maximum pressure peaks for $C = 10^2$ and $C = 10^5$ are larger than 3000 bar which are not in the range of depicted plot. Actually, most of the local peaks in the pressure profile can be regarded as spurious numerical pulses and it can be further distinguished if the plotted data are filtered out every 10 time steps as shown in Fig. 21b. From this figure, the finite mass transfer result for $C = 10^5$ is rather similar to the equilibrium model, although there is a time shift due to earlier collapse of the finite mass transfer approach. However, in general cases that the correct

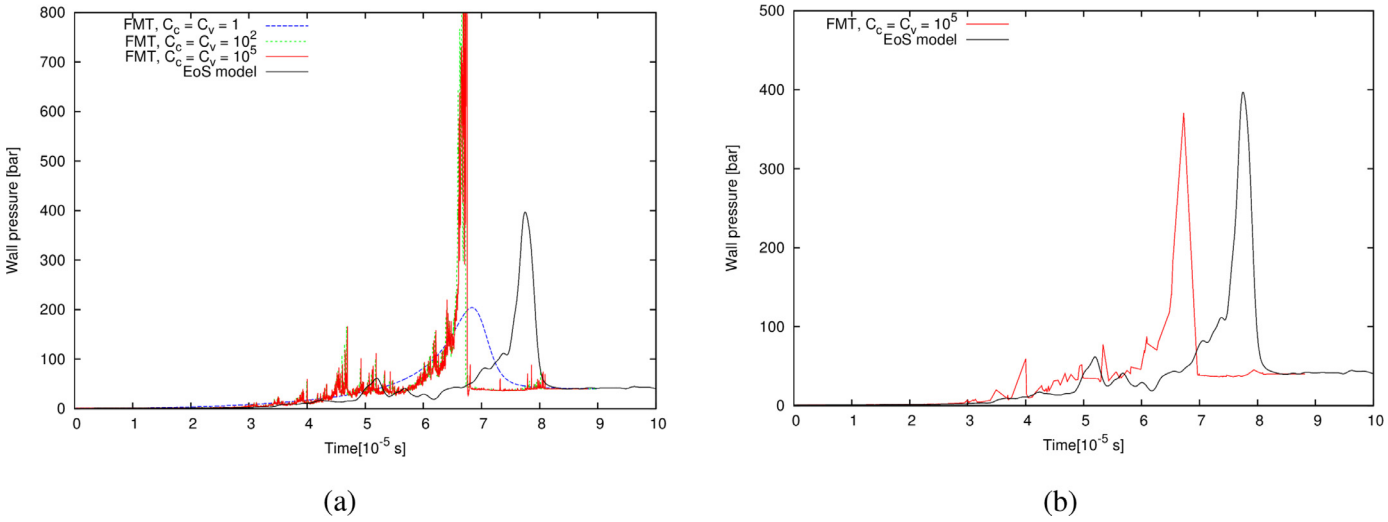

Fig. 21. Average wall pressure over the small transducer using finite mass transfer model; (a) comparison of different transfer coefficients; (b) filtered result with $C = 10^5$.

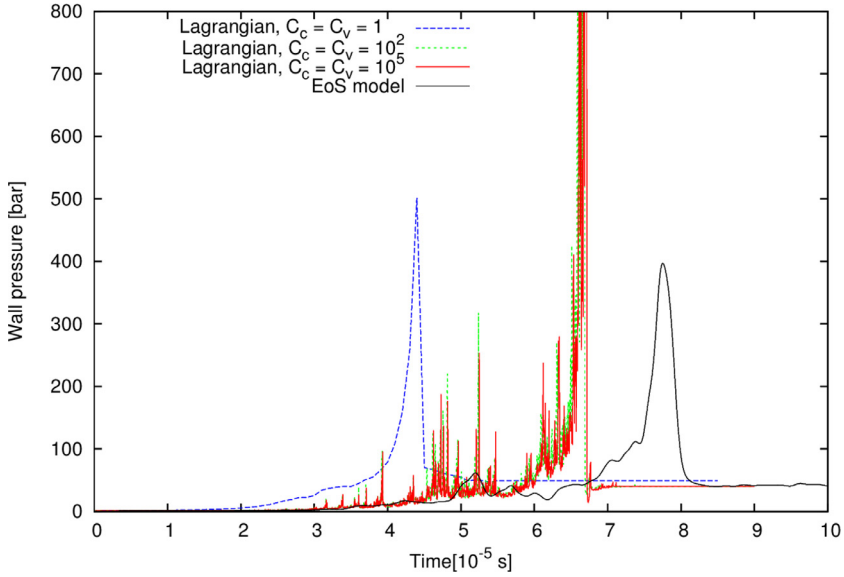

Fig. 22. Average wall pressure over the small transducer using Lagrangian model with different mass transfer coefficients.

solution is unknown, it is not possible to distinguish between numerical spurious peaks and physical collapse pulses and this can lead to inaccurate prediction of the impact loads and erosion estimations in cavitating flows.

In Fig. 22, the average pressure profiles of the Lagrangian model with localized R–P equation are compared with the equilibrium model result. It is seen that with small mass transfer coefficients, the bubble cloud collapses too early. As shown in Fig. 21a for the finite mass transfer model, when the empirical constants are small, the pressure field and its temporal peaks are not well captured. Since in the Lagrangian approach, the localized R-P solution is directly dependent on the surrounding pressure, an inaccurate pressure estimation leads to a wrong prediction of the vapour volume profile and collapse time. Also, for the larger coefficients, the estimated average pressures are similar to those of the finite mass transfer model, which shows that even with more accurate formulation in modelling the vapour interface, the numerical pulses still exist. As stated before, in this study the compressibility of pure liquid and vapour are not taken into account and it seems that the liquid incompressibility around the cloud is the major reason for spurious pulses. In an incompressible fluid, every single pulse from the variation of a bubble size appears as a sudden and simultaneous pressure change in the whole flow domain, including the wall boundary. Such numerical peaks can be seen in the work of Yakubov et al. (2015), where ignoring the pure phase compressibility caused quite larger peaks in the hydrofoil surface pressure and lift force profiles (Fig. 17 of Yakubov et al., 2015). However, considering the liquid compressibility in pressure based cavitating flow solvers may lead to ill-conditioned matrices of coefficients which needs special measures and smaller time steps to ensure solution stability and this, in turn increases the computational expenses; such an improvement is the subject of a future study.

For further comparison and understanding of different models, the bubble cloud structure and wall pressure contours at different time instances are depicted in Fig. 23. It should be noticed that the time instances of different rows of the figure are not exactly the same. Since the equilibrium model result has a small time delay as compared to the other two models (Figs. 19 and 20) the time instances of the equilibrium model contours are chosen a little later (0.2–0.4 μs) to compare the corresponding instances of cavity structures in each row. Also, since there is a 1 μs time difference in the collapse profile of the current equilibrium model re-

Please cite this article as: E. Ghahramani et al., A comparative study between numerical methods in simulation of cavitating bubbles, International Journal of Multiphase Flow (2018), https://doi.org/10.1016/j.ijmultiphaseflow.2018.10.010

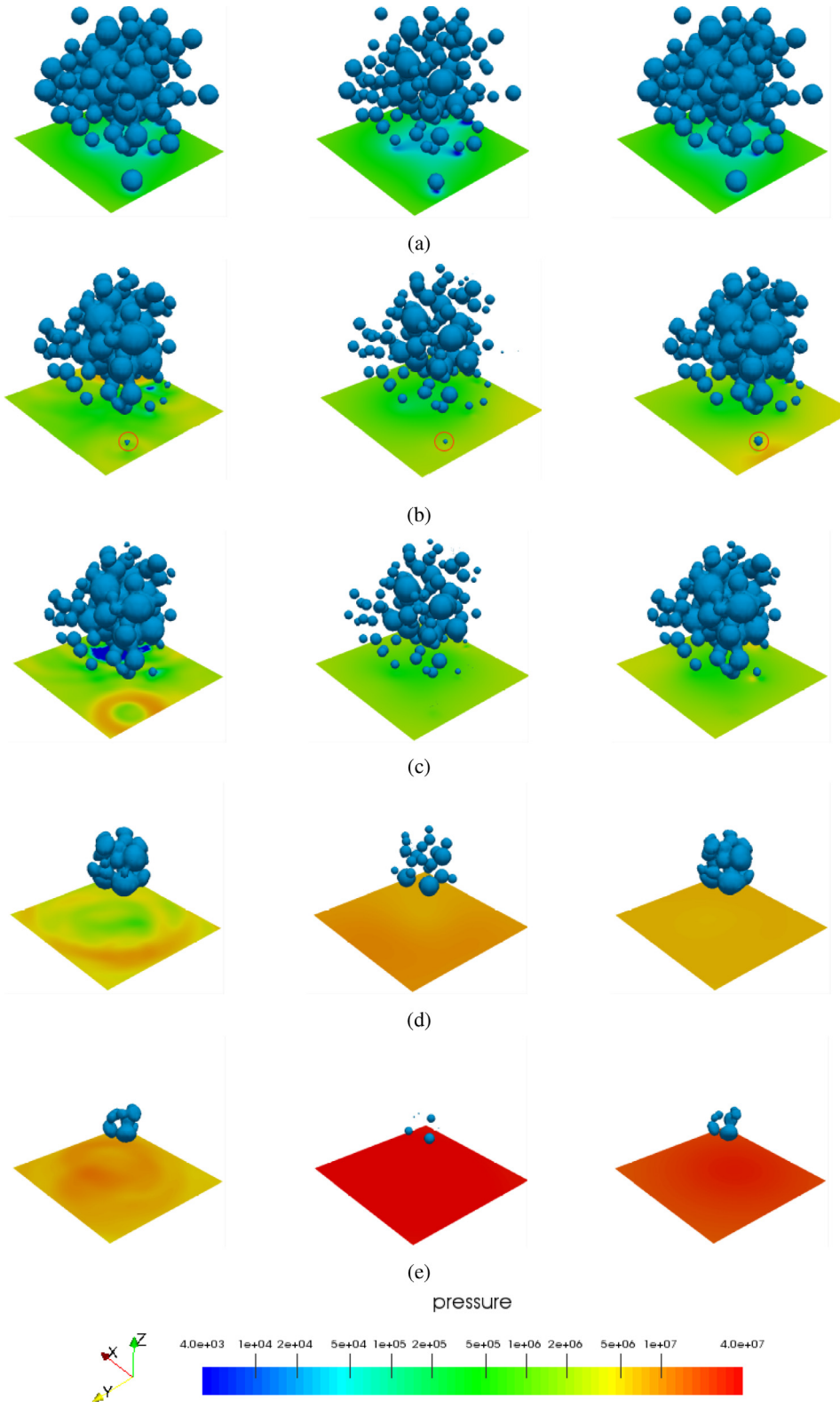

Fig. 23. Comparison of equilibrium model (left), Lagrangian model (middle) and finite mass transfer model (right) in prediction of cloud structure and wall pressure at different time instances (a) $t = 0$; (b) $t = 3.4$ μs; (c) $t = 3.7$ μs; (d) $t = 6.1$ μs; (e) $t = 6.8$ μs. (For interpretation of the references to colour in this figure legend, the reader is referred to the web version of this article.)

Please cite this article as: E. Ghahramani et al., A comparative study between numerical methods in simulation of cavitating bubbles, International Journal of Multiphase Flow (2018), https://doi.org/10.1016/j.ijmultiphaseflow.2018.10.010

sults and the corresponding data of Schmidt et al. (2011), the chosen time steps of Figs. 23c–e for the equilibrium model is about 1 μs larger than the corresponding values in Figs. 6(2)–6(4) of Schmidt et al. (2011). For plotting the cavity structures of the Eulerian models, the vapour fraction threshold of $0.01 < \alpha_v < 0.9$ is chosen. In Fig. 23a, it is seen that while in the Lagrangian approach each spherical bubble can be presented with the exact dimension, in the Eulerian modelling the vapour volume is distributed over a number cells which may lead to the diffusion of the bubble interface. For a more precise representation of bubble interfaces, a finer grid is needed as the one in the work of Schmidt et al. (2011) with 11 million cells in the inner domain or even, to have a better representation, the generated grid with a total of 120 million cells in the study of Adams and Schmidt (2013). Fig. 23b is depicted to show the similarity in the cavity structures despite the difference in estimation of the pressure profiles between the compressible and incompressible methods. The small marked bubble in this figure collapses a few time step later and since it is close to the bottom boundary, the collapse pressure effect on the wall is considerable. Based on Fig. 23c the equilibrium model can capture the emitted pressure wave on the wall as in this model the compressibility of the pure phases is taken into account. However, for the Lagrangian and finite mass transfer model the collapse pressure appears as a sudden and simultaneous pressure change in the whole flow domain (and not as an emitted wave). Therefore, no circular wave pattern is seen in the pressure contours of these models in which the liquid compressibility is neglected. In fact, the pressure on the wall, and specially close to collapse point, has a huge and instantaneous increase at the collapse time, but after just a few time steps the wall pressure becomes rather uniform.

Due to the non-symmetrical pressure field around the bubbles, they are expected to lose their spherical symmetry during the collapse, as predicted by the equilibrium model. In fact, in the last steps of the collapse, the bubbles are deformed by impinging liquid jets and they are finally pierced and take a torus shape. However, as shown in Fig. 23d for the Eulerian models, the bubbles have small deformation in shape while in the corresponding contours of Schmidt et al. (2011) (figure 6(3) of the paper) the small bubbles are already pierced by the liquid jet. The collapsing bubble have similar shapes later in Fig. 23e, while in Fig. 6(4) of Schmidt et al. (2011) (the corresponding instance) the last bubbles have torus shape. Therefore, the Eulerian equilibrium model, at least, can estimate the bubble piercing and non-symmetrical shapes, however it needs a very fine grid (around 220^3 cells for this case). From the middle contours of Figs. 23d and e, it is seen that the Lagrangian bubble stay spherical during the entire collapse time as in the Rayleigh–Plesset equation, the bubble is assumed to keep its symmetrical shape. However, it is possible to improve the Lagrangian model and consider the non-spherical shapes in this approach regardless of the computational grid size and it can be the subject of a future study.

5. Conclusions and future works

In this study, the performance of three different numerical models are compared by investigating two benchmark test cases, including a discussion on the effect of pressure computation approaches for the Lagrangian model. For the equilibrium model, the (pure phase) compressibility was taken into account by solving the corresponding equation of state for each phase and using a density-based algorithm. However, for the finite mass transfer model and the Lagrangian model, the pure fluid was assumed to be incompressible and a pressure based algorithm was used to consider pressure-velocity coupling. Also, in the Lagrangian model, the continuum fluid is solved similar to the finite mass transfer approach, however the cavities are represented by individual discrete bubbles. In this method, the bubble deformation was calculated using the original and improved forms of the Rayleigh–Plesset equation to investigate the effect of local pressure in estimation of bubble collapse rate. The first test case was the Rayleigh collapse problem, for which exact analytical results are available, to investigate the behaviour of each method for a fundamental problem. The second studied case was the collapse of a cloud of bubbles in which the flow field around each bubble was unsymmetric and the correct estimation of the local pressure plays a more important role. Finally, from the obtained results, the following conclusions are drawn:

- Both Eulerian models estimate a diffusive liquid–vapour interface and to have a more precise representation they need finer grids as compared to the Lagrangian model. The interface diffusivity can have considerable effect in the estimation of local pressure on the interface (as in the case of single bubble collapse) and the shape of cavity structure (as in the case of bubble cluster), especially in the last stages of the collapse.
- Some numerical pulses are detected in the estimated pressure profiles of the Eulerian models for the single bubble collapse problem, and this can be significant in collapse pressure calculation for special situations. From the comparison of the finite mass transfer and Lagrangian results, it is concluded that when the sharp bubble interface is estimated precisely, these numerical issues are solved.
- The numerical pulses are augmented when the grid lines are aligned with the bubble interface and there is a simultaneous phase change in several neighbouring cells. For the more complex case of bubble cluster, the Cartesian grid was used. Therefore, the pulses are not augmented, and they are negligible as compared to the high pressure in the farfield and large physical pressure peaks from individual bubble collapses.
- The Lagrangian models can give satisfactory results with larger time steps and coarser grids as compared to the Eulerian approaches.
- In the general cases that a bubble is surrounded by other cavity structures or confined by flow boundaries and the surrounding flow field is not symmetrical, it is necessary to use the local pressure in the R–P equation. The introduced localized Rayleigh–Plesset equation was shown to have a more appropriate representation of the bubble dynamics as compared to the original form of the equation or the above-mentioned improvements in the literature.
- The fluid compressibility is an effective parameter in estimation of the flow pressure and to have a reliable study of the cavity collapse pressure it is necessary to consider this parameter. However, from the comparison of the cavity structures of the compressible and incompressible simulation, it is seen that even by ignoring the fluid compressibility, the collapse rate and vapour distribution can be predicted with reasonable accuracy.

Also, it was shown that for the case of single bubble collapse, the Lagrangian model yields better accuracy compared to the finite mass transfer model, even with larger time steps and coarser grid cells. And for the more complicated case of bubble cluster the two approaches have similar accuracy. There are special problems in which the non-condensable gas content as well as fluid viscosity effects should be considered and these parameters are easier to implement in the R–P equation of the Lagrangian models as compared to the mass transfer source terms. Therefore, the Lagrangian model or a hybrid Eulerian–Lagrangian model can be suitable alternatives to the Eulerian finite mass transfer rate models. Development of a hybrid model is the subject of future studies. The implementation of the non-condensable gas effect in the compressible equilibrium is possible as well, however, it is not as straightforward as adding an additional term in the R–P equation. In ad-

Please cite this article as: E. Ghahramani et al., A comparative study between numerical methods in simulation of cavitating bubbles, International Journal of Multiphase Flow (2018), https://doi.org/10.1016/j.ijmultiphaseflow.2018.10.010

dition, the incompressible models should be improved to consider the pure phase compressibility for a more appropriate estimation of the pressure field. This development improves the generated pressure pulse and erosion estimation as well as solution of the localized Rayleigh–Plesset equation. Finally, for the special applications in which the bubble non-spherical shape at the latest stages of collapse is important, the effect of flow field unsymmetry can be further considered in the Lagrangian equations to improve the Lagrangian or hybrid model in this regard as well. For the pure Eulerian approaches more refined grids are needed to have an accurate estimation of the bubble shape, which makes the simulations limited to the small scale flow field, especially for the compressible density-based models.

Acknowledgements

This work is funded through the EU H2020 project CaFE, a Marie Skłodowska-Curie Action Innovative Training Network project, grant number 642536. The computations were performed partly on resources at Chalmers Centre for Computational Sciences and Engineering (C3SE) provided by the Swedish National Infrastructure for Computing (SNIC) and partly using resources provided by Leibniz Rechenzentrum (LRZ) at TU Munich. The authors wish to express their gratitude to Dr. Steffen Schmidt (TU Munich) for sharing the bubble cluster test case data and his research group for hosting Ebrahim Ghahramani in a two-month study visit as a part of the CaFE project. We further greatly appreciate the interesting discussion about the finite mass transfer models with Sören Schenke (TU Delft), who also kindly provided us with the generated grid for the bubble cluster test case.

References

Abdel-Maksoud, M., Hänel, D., Lantermann, U., 2010. Modeling and computation of cavitation in vortical flow. Int. J. Heat Fluid Flow 31 (6), 1065–1074.
Adams, N.A., Schmidt, S.J., 2013. Shocks in cavitating flows. Bubble Dyn.Shock Waves 235–256.
Asnaghi, A., Feymark, A., Bensow, R., 2017. Improvement of cavitation mass transfer modeling based on local flow properties. Int. J. Multiphase Flow 93, 142–157.
Barton, I.E., 1998. Comparison of simple-and piso-type algorithms for transient flows. Int. J. Numer. Methods Fluids 26 (4), 459–483.
Bensow, R.E., Bark, G., 2010. Implicit les predictions of the cavitating flow on a propeller. J. Fluids Eng. 132 (4), 041302.
Brennen, C.E., 2013. Cavitation and Bubble Dynamics. Cambridge University Press.
Eskilsson, C., Bensow, R., 2012. A compressible model for cavitating flow: comparison between euler, rans and les simulations. 29th Symposium on Naval Hydrodynamics, Gothenburg, Sweden.
Franc, J.-P., Michel, J.-M., 2006. Fundamentals of Cavitation, 76. Springer Science & Business Media.
Ghahramani, E., Arabnejad, M.H., Bensow, R., 2017. A hybrid model for simulation of cavitating flows. 12th OpenFOAM Workshop, University of Exeter, UK, 24–27 July.
Ghahramani, E., Arabnejad, M.H., Bensow, R.E., 2018. Realizability improvements to a hybrid mixture-bubble model for simulation of cavitating flows. Comput. Fluids doi:10.1016/j.compfluid.2018.06.025.
Giannadakis, E., 2005. Modelling of Cavitation in Automotive Fuel Injector Nozzles. Imperial College, University of London Ph.D. thesis.
Giannadakis, E., Gavaises, M., Arcoumanis, C., 2008. Modelling of cavitation in diesel injector nozzles. J. Fluid Mech. 616, 153–193.
Goncalves, E., Champagnac, M., Fortes Patella, R., 2010. Comparison of numerical solvers for cavitating flows. Int. J. Comput. Fluid Dyn. 24 (6), 201–216.
Hsiao, C.-T., Chahine, G.L., Liu, H.-L., 2000. Scaling effects on bubble dynamics in a tip vortex flow: prediction of cavitation inception and noise. Rep. 98007-1NSWC. Dynaflow Inc.
Hsiao, C.-T., Ma, J., Chahine, G.L., 2017. Multiscale tow-phase flow modeling of sheet and cloud cavitation. Int. J. Multiphase Flow 90, 102–117.
Ibsen, S., Schutt, C.E., Esener, S., 2013. Microbubble-mediated ultrasound therapy: a review of its potential in cancer treatment. Drug Des. Dev. Ther. 7, 375.
Koop, A.H., 2008. Numerical simulation of unsteady three-dimensional sheet cavitation Ph.D. thesis.
Koukouvinis, P., Gavaises, M., 2015. Simulation of throttle flow with two phase and single phase homogenous equilibrium model. In: Journal of Physics: Conference Series, 656. IOP Publishing, p. 012086.
Koukouvinis, P., Gavaises, M., Georgoulas, A., Marengo, M., 2016a. Compressible simulations of bubble dynamics with central-upwind schemes. Int. J. Comput. Fluid Dyn. 30 (2), 129–140.
Koukouvinis, P., Gavaises, M., Supponen, O., Farhat, M., 2016b. Numerical simulation of a collapsing bubble subject to gravity. Phys. Fluids 28 (3), 032110.
Koukouvinis, P., Gavaises, M., Supponen, O., Farhat, M., 2016c. Simulation of bubble expansion and collapse in the vicinity of a free surface. Phys. Fluids 28 (5), 052103.
Kunz, R.F., Boger, D.A., Stinebring, D.R., Chyczewski, T.S., Lindau, J.W., Gibeling, H.J., Venkateswaran, S., Govindan, T., 2000. A preconditioned navier–stokes method for two-phase flows with application to cavitation prediction. Comput. Fluids 29 (8), 849–875.
Kyriazis, N., Koukouvinis, P., Gavaises, M., 2017. Numerical investigation of bubble dynamics using tabulated data. Int. J. Multiphase Flow 93, 158–177.
Lauer, E., Hu, X., Hickel, S., Adams, N.A., 2012. Numerical modelling and investigation of symmetric and asymmetric cavitation bubble dynamics. Comput. Fluids 69, 1–19.
Liu, A.B., Mather, D., Reitz, R.D., 1993. Modeling the effects of drop drag and breakup on fuel sprays. Technical Report. Wisconsin Univ-Madison Engine Research Center.
Mattson, M., Mahesh, K., 2012. A one-way coupled, Euler–Lagrangian simulation of bubble coalescence in a turbulent pipe flow. Int. J. Multiphase Flow 40, 68–82.
Mei, R., 1992. An approximate expression for the shear lift force on a spherical particle at finite reynolds number. Int. J. Multiphase Flow 18 (1), 145–147.
Merkle, C.L., Feng, J., Buelow, P.E.O., 1998. Computational modelling of the dynamics of sheet cavitation. In: Proc. of the 3rd Int. Symp. on Cavitation, Grenoble, France.
Ogloblina, D., Schmidt, S.J., Adams, N.A., 2017. Simulation and analysis of collapsing vapor-bubble clusters with special emphasis on potentially erosive impact loads at walls. Experimental Fluid Mechanics.
OpenFoam, 2018. The Open Source CFD Toolbox openfoam foundation. Accessed: 2018-01-15,http://www.openfoam.com.
Patankar, S.V., Spalding, D.B., 1983. A calculation procedure for heat, mass and momentum transfer in three-dimensional parabolic flows. In: Numerical Prediction of Flow, Heat Transfer, Turbulence and Combustion. Elsevier, pp. 54–73.
Plesset, M.S., Prosperetti, A., 1977. Bubble dynamics and cavitation. Annu. Rev. Fluid Mech. 9 (1), 145–185.
Saurel, R., Abgrall, R., 1999. A multiphase godunov method for compressible multifluid and multiphase flows. J. Comput. Phys. 150 (2), 425–467.
Saurel, R., Cocchi, P., Butler, P.B., 1999. Numerical study of cavitation in the wake of a hypervelocity underwater projectile. J. Propul. Power 15 (4), 513–522.
Schenke, S., van Terwisga, T.J., 2017. Simulating compressibility in cavitating flows with an incompressible mass transfer flow solver. In: Proc. of the Fifth International Symposium on Marine Propulsors, smp17, Espoo, Finland, 1, pp. 71–79.
Schmidt, S., Mihatsch, M., Thalhamer, M., Adams, N., 2011. Assessment of the prediction capability of a thermodynamic cavitation model for the collapse characteristics of a vapor-bubble cloud. WIMRC 3rd International Cavitation Forum. University of Warwick UK.
Schmidt, S.J., Mihatsch, M.S., Thalhamer, M., Adams, N.A., 2014. Assessment of erosion sensitive areas via compressible simulation of unsteady cavitating flows. In: Advanced Experimental and Numerical Techniques for Cavitation Erosion Prediction. Springer, pp. 329–344.
Schnerr, G.H., Sauer, J., 2001. Physical and numerical modeling of unsteady cavitation dynamics. Fourth International Conference on Multiphase Flow, New Orleans, USA, 1.
Schnerr, G.H., Sezal, I.H., Schmidt, S.J., 2008. Numerical investigation of three-dimensional cloud cavitation with special emphasis on collapse induced shock dynamics. Phys. Fluids 20 (4), 040703.
Sezal, I., 2012. Compressible dynamics of cavitating 3-D multi-phase flows Ph.D. thesis.
Shampine, L.F., Reichelt, M.W., 1997. The matlab ode suite. SIAM J.Sci.Comput. 18 (1), 1–22.
Singhal, A.K., Athavale, M.M., Li, H., Jiang, Y., 2002. Mathematical basis and validation of the full cavitation model. Trans.-Am. Soc. Mech.Eng. J. Fluids Eng. 124 (3), 617–624.
Ström, H., Sasic, S., Holm-Christensen, O., Shah, L.J., 2016. Atomizing industrial gas-liquid flows–development of an efficient hybrid vof-lpt numerical framework. Int. J. Heat Fluid Flow 62, 104–113.
Tiwari, A., Pantano, C., Freund, J., 2015. Growth-and-collapse dynamics of small bubble clusters near a wall. J. Fluid Mech. 775, 1–23.
Venkatakrishnan, V., 1995. Convergence to steady state solutions of the euler equations on unstructured grids with limiters. J. Comput. Phys. 118 (1), 120–130.
Wagner, W., Kretzschmar, H.-J., 2008. International steam tables-properties of water and steam based on the industrial formulation iapws-if97.
Wang, Y.-C., Brennen, C.E., 1999. Numerical computation of shock waves in a spherical cloud of cavitation bubbles. ASME J. Fluids Eng. 121 (4), 872–880.
Yakubov, S., Cankurt, B., Maquil, T., Schiller, P., Abdel-Maksoud, M., Rung, T., 2013. Advanced lagrangian approaches to cavitation modelling in marine applications. In: MARINE 2011, IV International Conference on Computational Methods in Marine Engineering. Springer, pp. 217–234.
Yakubov, S., Maquil, T., Rung, T., 2015. Experience using pressure-based cfd methods for euler–euler simulations of cavitating flows. Comput. Fluids 111, 91–104.
Ye, Y., Li, G., 2016. Modeling of hydrodynamic cavitating flows considering the bubble-bubble interaction. Int. J. Multiphase Flow 84, 155–164.